AD_____

Award Number: W81XWH-07-1-0171

TITLE: Robotic Prostate Biopsy in Closed MRI Scanner

PRINCIPAL INVESTIGATOR: Gregory Fischer

CONTRACTING ORGANIZATION: Johns Hopkins University
Baltimore, MD 21218

REPORT DATE: February 2008

TYPE OF REPORT: Annual Summary

PREPARED FOR: U.S. Army Medical Research and Materiel Command
Fort Detrick, Maryland 21702-5012

REPORT DOCUMENTATION PAGE

Form Approved
OMB No. 0704-0188

1. REPORT DATE	2. REPORT TYPE	3. DATES COVERED
14-02-2008	Annual Summary	15 JAN 2007 - 14 JAN 2008

4. TITLE AND SUBTITLE
Robotic Prostate Biopsy in Closed MRI Scanner

5a. CONTRACT NUMBER

5b. GRANT NUMBER
W81XWH-07-1-0171

5c. PROGRAM ELEMENT NUMBER

6. AUTHOR(S)
Gregory Fischer

Email: gfisch@jhu.edu

5d. PROJECT NUMBER

5e. TASK NUMBER

5f. WORK UNIT NUMBER

7. PERFORMING ORGANIZATION NAME(S) AND ADDRESS(ES)

Johns Hopkins University
Baltimore, MD 21218

8. PERFORMING ORGANIZATION REPORT NUMBER

9. SPONSORING / MONITORING AGENCY NAME(S) AND ADDRESS(ES)
U.S. Army Medical Research and Materiel Command
Fort Detrick, Maryland 21702-5012

10. SPONSOR/MONITOR'S ACRONYM(S)

11. SPONSOR/MONITOR'S REPORT NUMBER(S)

12. DISTRIBUTION / AVAILABILITY STATEMENT
Approved for Public Release; Distribution Unlimited

13. SUPPLEMENTARY NOTES

14. ABSTRACT

MRI possess many of the capabilities that TRUS is lacking for prostate brachytherapy and biopsy, with high sensitivity for detecting prostate tumors, high spatial resolution, excellent soft tissue contrast, and volumetric imaging capabilities. However, closed-bore high-field MRI has not been widely adopted for prostate interventions because strong magnetic fields and confined physical space present formidable challenges. This work enables prostate brachytherapy and biopsy procedures in standard high-field diagnostic MRI scanners through the development of a robotic needle placement device specifically designed for trans-perineal access to the prostate under real-time MR image guidance. Specifically, the requirements are defined, the system designed and constructed, the controller developed, and the full system evaluated in phantom models.

15. SUBJECT TERMS
Prostate, Biopsy, Brachytherapy, MRI, Robotic Surgery, Image Guided Surgery

16. SECURITY CLASSIFICATION OF:			17. LIMITATION OF ABSTRACT	18. NUMBER OF PAGES	19a. NAME OF RESPONSIBLE PERSON
a. REPORT	b. ABSTRACT	c. THIS PAGE			USAMRMC
U	U	U	UU	68	19b. TELEPHONE NUMBER *(include area code)*

Table of Contents

Page

Progress Report Summary
Project Year 1 (2007)

A. INTRODUCTION

Magnetic Resonance Imaging (MRI) is an excellent imaging modality for many conditions, but to date there has been limited success in harnessing this modality for the guidance of interventional procedures. MRI is an ideal interventional guidance modality: it provides near real-time high-resolution images at arbitrary orientations and is able to monitor therapeutic agents, surgical tools, biomechanical tissue properties, and physiological function. At the same time, MRI poses formidable engineering challenges by severely limited access to the patient and high magnetic field that prevents the use of conventional materials and electronic equipment. Currently, no technological solution exists to assist MRI guided prostate interventions in an accurate, simple, and economical manner. The objective of our research is to make conventional diagnostic closed high-field MRI scanners available for guiding prostatic needle placement interventions. My approach is to employ electro-mechanical devices for assisting clinicians with needle placement while taking advantage of real time MR images for guidance – the goal is to implement a remotely actuated robotic needle placement system in standard closed high-field magnets, optimized for transperineal prostate biopsy.

B. BODY

B.1. Brief System Concept

The system concept is shown in Fig. 1. The patient is positioned in the semi-lithotomy position for a trans-perineal approach to the prostate similar to traditional transrectal ultrasound (TRUS) based procedures. The robot is contained fully within the leg rest to provide a well defined workspace. The robot is controlled by pneumatic actuators, thus making the actuator fully MRI compatible. This allows real-time MRI images to provide guidance for the needle insertion procedures. The initial application is MRI-guided prostate, followed by prostate brachytherapy seed placement.

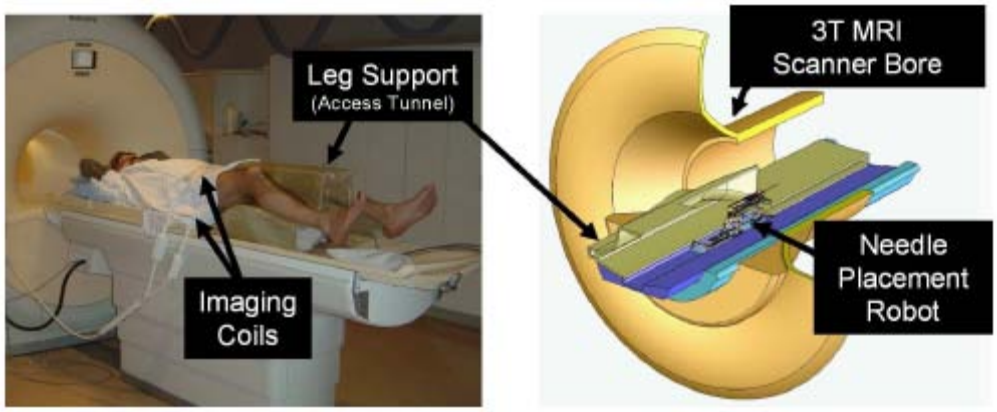

Figure 1: Proposed patient positioning in the semi-lithotomy position on the leg support (left) and robot position within the access tunnel (right). Access to the prostate is made through the perineal wall which rests against the superior surface of the leg rest.

B.2. Proposed Statement of Work (From initial proposal submission)

The detailed statement of work is as follows:

Aim-1: System Design will include an in depth study of the problem through collaboration with clinicians and other experts in the field, definition the available workspace and specific design requirements, and detailed design the robotic manipulator.

Aim-2: Robotic Assistant will be constructed for applications where real-time imaging is necessary but the physician does not have access to the patient inside the magnet. We will construct a 5 degree-of-freedom (DOF) robotic assistant and optimize it for transperineal prostate biopsy. MR-compatibility of materials and components will be evaluated, intermediate prototypes will be tested, design will be finalized, and the manipulator will be constructed.

Aim-3: Robot Control will be implemented in two phase: 1) low level control of the joints will allow required procedural accuracy and 2) high level control will incorporate real time MR imaging and tracking data to guide needle placement. The kinematics and dynamics of the robot will be analyzed, control algorithms will be compared and optimized, and systems integration will be performed. The complete system including robot, low level controller, high level controller, and MR imaging will be integrated together.

Aim-4: Validation of the system will verify the procedural accuracy of the integrated system including MR imaging and robot control. The functions of the device will be tested in phantom studies at the Brigham and Women's Hospital.

B.3. Progress Report for First Year

Aim-1: Detailed Design: Aim 1 focuses on the robotic assistant device design and system architecture. These have been developed in a collaborative manner with colleagues in the Surgical Planning Lab (SPL) at the Brigham and Women's Hospital (BWH). The detailed design requirements have been analyzed to optimize the system for trans-perineal prostate brachytherapy and biopsy. It was determined that 5 degrees of freedom (DOF) of motion are necessary for appropriate access to the prostate as shown in Fig. 2; these include two translational motions that effectively produce an automated template as in TRUS-guided procedures, and two rotational motions that enable needle orientations necessary for steering around the pubic arch or other obstacles [1,2]. The later set of motions truly sets this technique apart, because patients with large prostates that are typically contraindicated for the procedure can now be treated because of the increased access. The primary end effector will be a biopsy gun, with provisions for implementing a brachytherapy seed placement device or other needle driver at a later date.

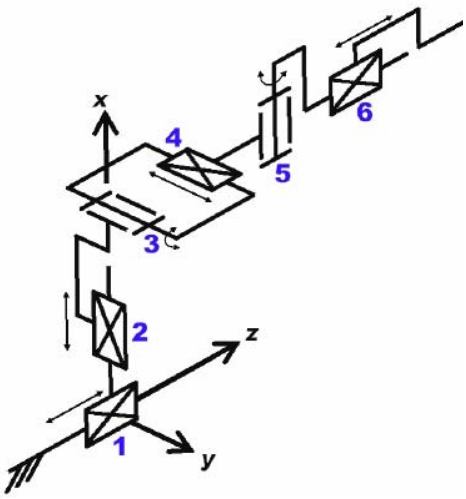

	Degree of Freedom	Motion	Requirements
1)	Gross Axial Position	1m	Manual with repeatable stop
2)	Vertical Motion	0-100mm	Precise servo control
3)	Elevation Angle	+15°, −0°	Precise servo control
4)	Horizontal Motion	±50mm	Precise servo control
5)	Azimuth Angle	±15°	Precise servo control
6)	Needle Insertion	150mm	Manual or Automated
7)	Canula Retraction or Biopsy Gun Firing	60mm	Manual or Automated
8)	Needle Rotation	360°	Manual or Automated

Fig. 2: The equivalent kinematic diagram and corresponding degrees of freedom of the robot developed based on the specific requirements for trans-perineal prostate biopsy and brachytherapy.

Aim-2: Robotic Manipulator: Aim 2 was focused on the development of the robotic needle placement assistant. The robot is actuated by air cylinders and location is monitored by optical encoders [1,2]. The manipulator is constructed of two planar mechanisms. The vertical mechanism takes the form of two sets of scissor mechanisms that provide vertical motion and optionally elevation angle. The horizontal mechanism is composed of two scott-russell mechanisms that provide horizontal translation and optionally azimuth angulation. The first prototype of the robotic manipulator has been constructed based upon the requirements shown in Fig. 3. This version is configured as an automated brachytherapy template with automated translation in the horizontal and vertical directions and an encoded insertion much like a grid-based procedure. The robot allows for higher positioning accuracy and the ability to perform the procedure inside the constraints of the MR scanner under real-time imaging.

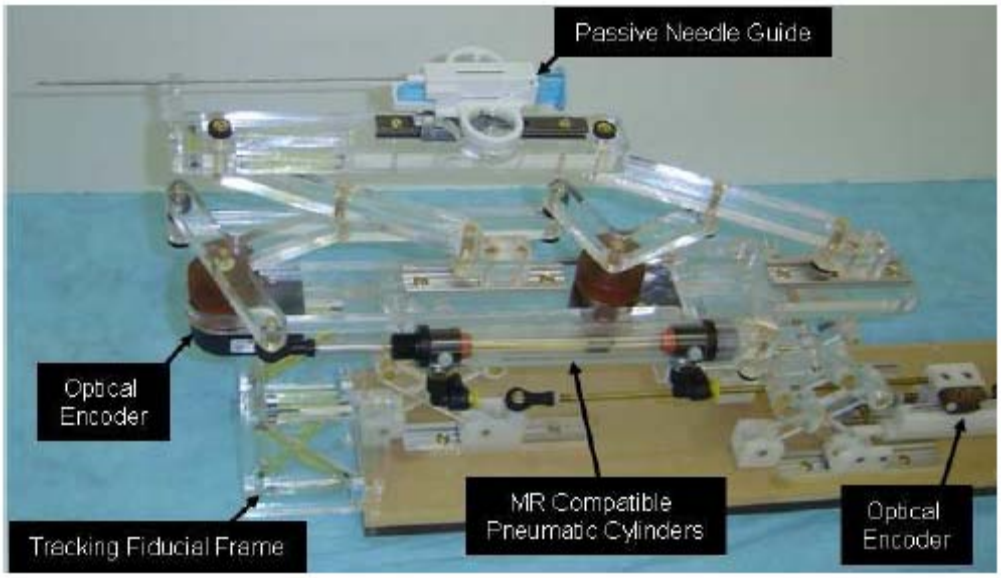

Fig. 3: The prototype robotic needle placement device configured with a biopsy needle end effector.

Aim-3: Robot Control: The goal of Aim 3 was to develop both the hardware and algorithms for accurate control of the pneumatically operated robot. The hardware for the system is complete. Fig. 4 shows the insides of the constructed robot controller. This controller sits inside the MRI scanner room during imaging near the foot of the bed. Inside is an embedded computer that communicates via a finer optic link to a planning and visualization workstation in the MR console room. The manipulator's air cylinders, shown in Fig.3, are controlled using piezoelectric servo valves. By designing a controller that can be used in the MR scanner room, the air hose lengths can be minimized, thus improving response time, smoothness, and accuracy of motion.

The second phase of Aim 3 is the control algorithms to make accurate control possible. Traditional control algorithms have been implemented on the system and are showing sufficient results to prove the concept. Detailed modeling of the mechanical system and the pneumatic system is underway. This will enable implementation of further novel control systems that promise high accuracy.

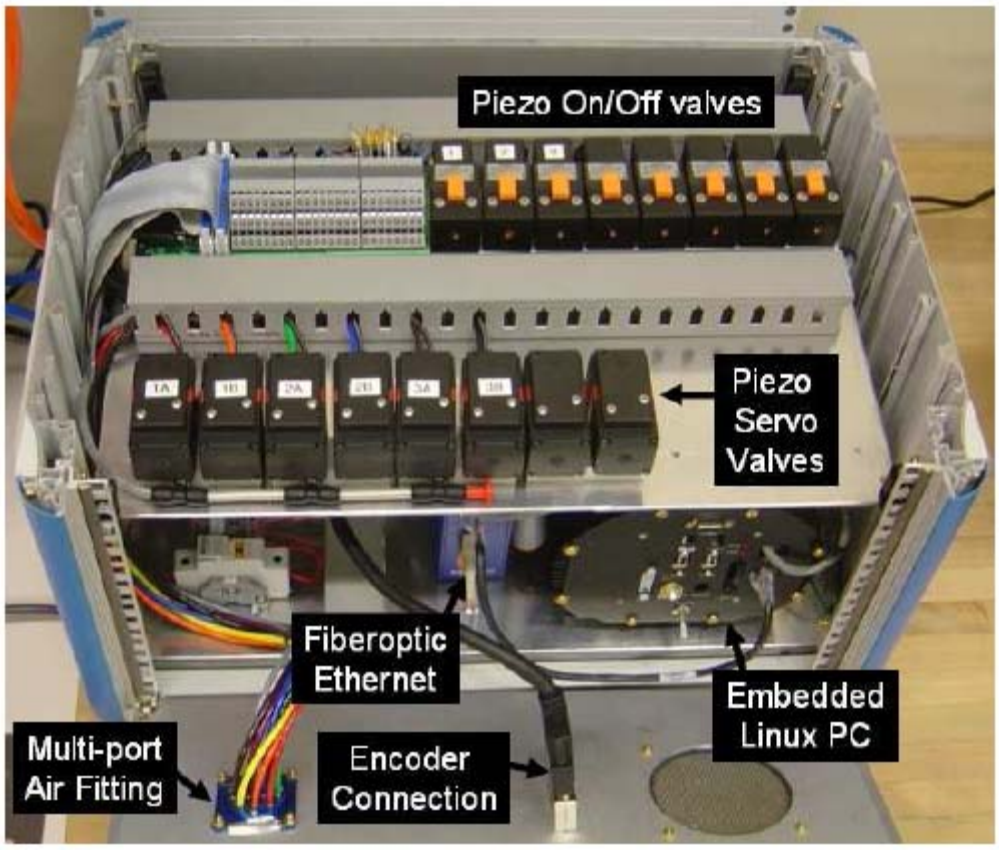

Fig. 4: The MRI-compatible robot controller incorporates an embedded computer, fiber optic communications, and piezoelectric valves, and operates inside the scanner room.

Aim-4: System Validation: The focus of Aim 4 is to ensure the system meets the requirements – this falls into two categories. First is the evaluation of the robot itself, and the second is evaluation of the complete integrated system as a whole. Thus far, both the robot and the system have undergone preliminary validation experiments. With the current control algorithms in place, the targeting accuracy of the robot is about 5mm – this represents the size of a clinically significant foci and the typical grid spacing of TRUS-guided procedures. With the enhanced control techniques from Aim 3 in place, accuracy is expected to be better than 1mm.

Fig. 5 shows an evaluation experiment of the system as a whole. This includes the MR scanner interface, the planning and visualization software [3,4], communications with the robot, tracking the robot [6], the robot controller, and the manipulator itself [1,2]. Experiments for targeting five 1cm objects in a tissue phantom proved successful. Further, the MR compatibility of the system has been thoroughly evaluated – losses in signal to noise ratio (SNR) have shown to be limited to 5% which implies that the system has no significant effect on image quality [5]. Currently, improvements are being made in all aspects of the system, and upcoming experiments are expected to provide promising results that justify moving into animal and cadaver trials.

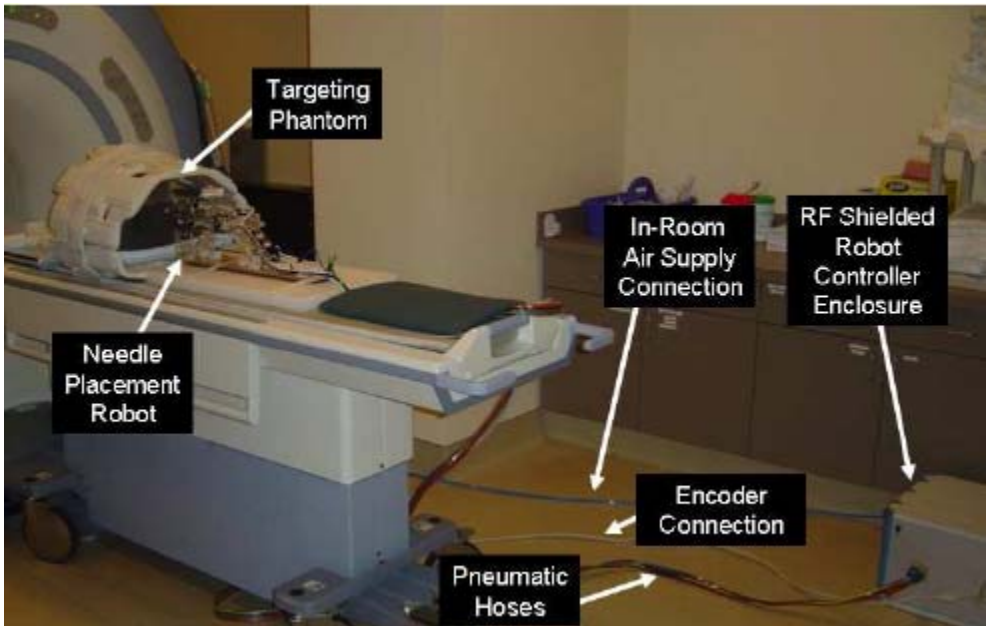

Fig. 5: Configuration of robot for system evaluation trials. The robot resides on the table at a realistic relative position to the phantom. The controller operates in the room at a distance of 3*m* from the 3T MRI scanner without functional difficulties or significant image quality degradation.

C. KEY RESEARCH ACCOMPLISHMENTS

- Development of MRI compatible robot controller
- Development of MRI compatible needle placement robot
- Integration of robot controller with planning software
- MRI compatibility evaluation of system
- Phantom studies for workflow evaluation
- Training of the PI

D. REPORTABLE OUTCOMES

Please see References section for publications resulting from this research.

No patent applications have been filed since the granting of this award.

This award supports the PI's Ph.D. dissertation research.

The PI is currently applying for faculty positions based in part upon experience and training received as part of this award

E. CONCLUSION

In conclusion, much of the proposed work has been completed to date, and the remainder is expected to be completed on schedule. The system's requirements have been finalized, the needle placement robot has been constructed, the controller hardware has been constructed, the controller software has been implements, system integration tests have been performed, MRI-compatibility has been validated, and initial system validation in phantom models has been completed. Future work includes further refining the controller to provide more accurate response, refining the software interface, and performing detailed analysis of the needle insertion accuracy and validation of the workflow.

so what: Over 40,000 brachytherapies are performed in the U.S. each year and the number is steadily growing. Transrectal Ultrasound (TRUS) is the current "gold standard" for guiding both biopsy and brachytherapy; however, TRUS-guided biopsy has a detection rate of only 20-30%, primarily due to the low sensitivity (60%) and poor positive predictive value (25%) of ultrasound. Furthermore, TRUS cannot effectively monitor the implant procedure as implanted seeds cannot be seen in the image. MRI seems to possess many of the capabilities that TRUS is lacking with high sensitivity for detecting prostate tumors, high spatial resolution, excellent soft tissue contrast, and volumetric imaging capabilities. However, closed-bore high-field MRI has not been widely adopted for prostate interventions because strong magnetic fields and confined physical space present formidable challenges. The significance of this work is to bring about the ability and practicality of performing prostate brachytherapy and biopsy procedures in standard high-field diagnostic MRI scanners.

G. REFERENCES (List of publications arising from the grant, sorted by publication date)

[1] **Fischer GS**, Iordachita I, Csoma C, Tokuda J, DiMaio SP, Tempany CM, Hata N, Fichtinger G, MRI-Compatible Pneumatic Robot for Transperineal Prostate Needle Placement, IEEE / ASME Transactions on Mechatronics – Focused section on MRI Compatible Mechatronic Systems, June 2008 (In Press)

[2] **Fischer GS**, Iordachita I, Csoma C, Tokuda J, Mewes PW, Tempany CM, Hata N, Fichtinger G, Pneumatically Operated MRI-Compatible Needle Placement Robot for Prostate Interventions, International Conference on Robotics and Automation - ICRA 2008, Pasadena, CA, May 2008 (Accepted)

[3] Mewes PW, Tokuda J, DiMaio SP, **Fischer GS**, Csoma C, Gobbi DG, Tempany CM, Fichtinger G, Hata N, An Integrated MRI and Robot Control Software for an MRI-compatible Robot in Prostate Intervention, International Conference on Robotics and Automation - ICRA 2008, Pasadena, CA, May 2008 (Accepted)

[4] Tokuda J, DiMaio SP, **Fischer GS**, Csoma C, Gobbi D, Fichtinger G, Hata N, Tempany CM, Real-time MR Imaging Controlled by Transperineal Needle Placement Device for MRI-guided Prostate Biopsy, 16th Scientific Meeting and Exhibition of the International Society of Magnetic Resonance in Medicine - ISMRM 2008, Toronto, Canada, May 2008 (Accepted)

[5] **Fischer GS**, Iordachita I, DiMaio SP, Fichtinger G, Development of a Robotic Assistant for Needle-Based Transperineal Prostate Interventions in MRI, 10th International Conference on Medical Image Computing and Computer-Assisted Intervention - MICCAI 2007, Brisbane, Australia, Vol 1, pp 425-453, November 2007

[6] DiMaio SP, Samset E, **Fischer GS**, Iordachita I, Fichtinger G, Jolesz F, Tempany C, Dynamic MRI Scan Plane Control for Passive Tracking of Instruments and Devices, 10th International Conference on Medical Image Computing and Computer-Assisted Intervention - MICCAI 2007, Brisbane, Australia, Vol 2, pp 50-58, November 2007

F. APPENDICES

- "MRI-Compatible Pneumatic Robot for Transperineal Prostate Needle Placement" prepared for IEEE / ASME Transactions on Mechatronics, June 2008
- "Pneumatically Operated MRI-Compatible Needle Placement Robot for Prostate Interventions" prepared for the International Conference on Robotics and Automation, May 2008
- "Development of a Robotic Assistant for Needle-Based Transperineal Prostate Interventions in MRI" prepared for the 10th International Conference on Medical Image Computing and Computer-Assisted Intervention, November 2007

MRI-Compatible Pneumatic Robot for Transperineal Prostate Needle Placement

Gregory S. Fischer[1], Iulian Iordachita[1], Csaba Csoma[1],
Junichi Tokuda[2], Simon P. DiMaio[2],
Clare M. Tempany[2], Nobuhiko Hata[2] and Gabor Fichtinger[1,3]

[1] Johns Hopkins University, Baltimore, MD, USA
[2] Brigham and Women's Hospital, Boston, MA,USA
[3] Queen's University, Kingston, Ontario, Canada

Corresponding Author:
Gregory Fischer
3400 N. Charles St., CSEB-B08B
Baltimore, MD 21218
Phone: (410)516-4723
Fax: (410)516-3332
gfischer@jhu.edu

Submitted to the:
Focused Section on MRI Compatible Mechatronic Systems
IEEE/ASME Transactions on Mechatronics

Keywords: MRI-Compatible Robotics,
Pneumatic Control, Prostate Brachytherapy and Biopsy

December 3, 2007

Abstract

Magnetic Resonance Imaging (MRI) can provide high-quality 3D visualization of prostate and surrounding tissue, thus granting potential to be a superior medical imaging modality for guiding and monitoring prostatic interventions. However, the benefits can not be readily harnessed for interventional procedures due to difficulties that surround the use of high-field (1.5T or greater) MRI. The inability to use conventional mechatronics and the confined physical space make it extremely challenging to access the patient. We have designed a robotic assistant system that overcomes these difficulties and promises safe and reliable intra-prostatic needle placement inside closed high-field MRI scanners. MRI compatibility of the robot has been evaluated under 3T MRI using standard prostate imaging sequences and average SNR loss is limited to 5%. The complete system workflow has been evaluated in phantom studies with accurate visualization and targeting of five out of five $1cm$ targets. The paper explains the robot mechanism and controller design, the system integration, and presents results of preliminary evaluation of the system.

1 Introduction

Each year approximately 1.5 million core needle biopsies are performed, yielding about 220,000 new prostate cancer cases in the U.S. [1]. If the cancer is confined to the prostate, then low-dose-rate (LDR) permanent brachytherapy is a common treatment option; a large number (50-150) of radioactive pellets/seeds are implanted into the prostate using 15-$20cm$ long 18G needles [2]. A complex seed distribution pattern must be achieved with great accuracy in order to eradicate the cancer, while minimizing radiation toxicity to adjacent healthy tissues. Over 40,000 brachyther-

apies are performed in the U.S. each year and the number is steadily growing [3]. Transrectal Ultrasound (TRUS) is the current "gold standard" for guiding both biopsy and brachytherapy due to its real-time nature, low cost, and apparent ease of use [4]. However, TRUS-guided biopsy has a detection rate of only 20-30% [5], primarily due to the low sensitivity (60%) and poor positive predictive value (25%) of ultrasound [6]. Furthermore, TRUS cannot effectively monitor the implant procedure as implanted seeds cannot be seen in the image. MRI seems to possess many of the capabilities that TRUS is lacking with high sensitivity for detecting prostate tumors, high spatial resolution, excellent soft tissue contrast, and volumetric imaging capabilities. However, closed-bore high-field MRI has not been widely adopted for prostate interventions because strong magnetic fields and confined physical space present formidable challenges.

The clinical efficacy of MRI-guided prostate brachytherapy and biopsy was demonstrated by D'Amico, Tempany, et al. at the Brigham and Women's Hospital using a 0.5T open-MRI scanner [7, 8]. MR images were used to plan and monitor transperineal needle placement. The needles were inserted manually using a guide comprising a grid of holes, with the patient in the lithotomy position, similarly to the TRUS-guided approach. Zangos et al. used a transgluteal approach with 0.2T MRI, but did not specifically target the tumor foci [9]. Susil et al. described four cases of transperineal prostate biopsy in a closed-bore scanner, where the patient was moved out of the bore for needle insertions and then placed back into the bore to confirm satisfactory placement [10]. Beyersdorff et al. performed targeted transrectal biopsy in a 1.5T MRI unit with a passive articulated needle-guide and have reported 12 cases of biopsy to date [11].

A thorough review of MRI compatible systems to date for image guided interventions by

Tsekos et al. can be found in [12]. Robotic assistance has been investigated for guiding instrument placement in MRI, beginning with neurosurgery [13] and later percutaneous interventions [14, 15]. Chinzei et al. developed a general-purpose robotic assistant for open MRI [16] that was subsequently adapted for transperineal intra-prostatic needle placement [17]. Krieger et al. presented a 2-DOF passive, un-encoded and manually manipulated mechanical linkage to aim a needle guide for transrectal prostate biopsy with MRI guidance [18]. With the use of three active tracking coils, the device is visually servoed into position and then the patient is moved out of the scanner for needle insertion.

Developments in MR compatible motor technologies include Stoianovici et al. who describes a fully MRI compatible pneumatic stepper motor called PneuStep in [19], Elhawary et al. who describes an air motor for limb localization in [20] and Zaman et al. who describes a stepper motor that uses the scanner's magnetic field as a driving force is described in [21]. Other recent developments in MRI-compatible mechanisms include pneumatic stepping motors on a light needle puncture robot [22] and haptic interfaces for fMRI [23]. Ultrasonic Motor drive techniques that enhance MR compatibility are described by Suzuki et al. in [24], and the feasibility of using piezoceramic motors for robotic prostate biopsy is presented in [25]. Stoianovici et al. have taken their developments in MR-compatible pneumatic stepper motors and applied them to robotic brachytherapy seed placement [26]. This system is fully MR-compatible, fully automatic prostate brachytherapy seed placement system; the patient is in the decubitus position and seeds are placed in the prostate transperineally. The relatively high cost and complexity of the system, in addition to the requirement to perform the procedure in a different pose than used for preoperative imaging

are issues that we intend to overcome with the work presented here.

This work introduces the design of a novel computer-integrated robotic mechanism for transperineal prostate needle placement in 3T closed-bore MRI. The mechanism is capable of positioning the needle for the purposes of treatment by ejecting radioactive seeds, or diagnosis by harvesting tissue samples inside the magnet bore. The robot operates under remote control of the physician without moving the patient from the imaging space. This enables the use of real-time imaging for precise placement of needles in soft tissues. In addition to structural images, protocols for diffusion imaging and MR spectroscopy will be available intraoperatively, promising enhanced visualization and targeting of pathologies. Accurate and robust needle placement devices, navigated based on such image guidance, are becoming invaluable clinical tools and have clear applications in several other organ systems.

The full system architecture, including details regarding planning software and integration of real-time MR imaging are described in [27]. This focus of this paper is design and evaluation of the robotic needle placement manipulator and is organized as follows: Section 2 describes the workspace analysis and design requirements for the proposed device, while Section 3 describes the detailed design of system prototype. Results of the MR compatibility, workflow validation and accuracy are presented in Section 4, with a discussion of the system and future plans in Section 5.

2 Design Requirements

2.1 Workspace Analysis

The system's principal function is accurate needle placement in the prostate for diagnosis and treatment, primarily in the form of biopsy and brachytherapy seed placement respectively. In our

approach, the patient is positioned in the supine position with the legs spread and raised as shown in Fig. 1 (left). The patient is in a similar configuration to that of TRUS-guided brachytherapy, but the MRI bore's constraint ($60cm$ diameter) necessitates that the legs be spread less and the knees be lowered into a semi-lithotomy position. The robot operates in the confined space between the patient's legs without interference with the patient, MRI scanner components, anesthesia equipment, and auxiliary equipment present as shown in the cross-section shown in Fig. 1 (right).

The average size of the prostate is $50mm$ in the lateral direction by $35mm$ in the anterior-posterior direction by $40mm$ in length. The volume of the prostate volume can be approximated by an elliptical volume formula of the form $V = (.525 \times D_1 \times D_2 \times D_3)$, and the average volume is about $35cc$. By the end of a procedure, the volume of the prostate can also enlarge by 25% due to swelling [28]. For our system, the standard $60mm \times 60mm$ perineal window of TRUS-guided brachytherapy was increased to $100mm \times 100mm$, in order to accommodate patient variability and lateral asymmetries in patient setup. In depth, the workspace extends to $150mm$ superior of the perineal surface. Direct access to all clinically relevant locations in the prostate is not always possible with a needle inserted purely along apex-base direction due to pubic arch interference (PAI). If more than 25% of the prostate diameter is blocked (typically in prostates larger than $55cc$), then the patient is usually declined for implantation [28]. The addition needle angulation in the sagittal and coronal planes in the proposed system will enable procedure to be performed on many of these patients who are typically contraindicated for brachytherapy due to PAI.

2.2 System Requirements

The kinematic requirements of the robot are derived from the workspace analysis. A kinematic diagram of the proposed system is shown in Fig. 2. The primary actuated motions of the robot include two prismatic motions and two rotational motions. The robot is situated upon a manual linear slide that positions the robot in the access tunnel and allows fast removal for reloading brachytherapy needles or collecting harvested biopsy tissue. Additional application-specific motions are also required; these include needle insertion, canula retraction, needle rotation, and biopsy gun actuation. The accuracy of the individual servo controlled joints is targeted to be $0.1mm$, and the needle placement accuracy of the robot is targeted to be $0.5mm$. This target accuracy approximates the voxel size of the MR images used, which represents the finest possible targeting precision.

The overall system accuracy, however, is expected to be somewhat less when effects such as imaging resolution, needle deflection, and tissue deformation are taken into account. The specifications for the requirements of each motion are shown in Table 1. The numbered motions in the table correspond to the labeled joints in the equivalent kinematic diagram shown in Fig. 2. $DOF\#1$-6 represent the primary robot motions and $DOF\#7\&8$ represent application-specific motions. These specifications represent a flexible system that can accommodate a large variety of patients.

2.3 MRI Compatibility Requirements

Design of a system operating inside the bore of a high-field 1.5-$3T$ MRI scanner adds significant complexity since traditional mechatronics materials, sensors and actuators cannot be employed. In order for a device to be MR compatible, it must be MR safe, not compromise image quality and

not be affected by the scanner's electric and magnetic fields [16]. Ferromagnetic materials must be avoided entirely because they cause image artifacts and distortion due to field inhomogeneities, and can pose a dangerous projectile risk. Non-ferromagnetic metals such as aluminum, brass, and titanium or high strength plastic and composite materials are therefore permissible. However, the use of any conductive materials in the vicinity of the scanner's isocenter must be limited because of the potential for induced eddy currents to disrupt the magnetic field homogeneity. To prevent or limit local heating in the proximity of the patient's body, the materials and structures used must be either non-conductive or free of loops and of carefully chosen lengths to avoid eddy currents and resonance. In this robot, all electrical and metallic components are isolated from the patient's body. The following section details material and component selection, with the consideration of MRI compatibility issues.

3 System and Component Design

3.1 Overview

Not all of the DOF listed in Table 1 are necessary for the initial proof-of-concept system and Phase-1 clinical trials. The first embodiment of the system provides the two prismatic motions in the axial (transverse) plane over the perineum ($DOF\#2$ and $DOF\#4$) and an encoded manual needle guide ($DOF\#6$). This represents an automated high-resolution needle guide, functionally similar to the template used in conventional brachytherapy. The next design iteration will produce a 4-DOF robot base that includes the two angulation DOFs. The 4-DOF base of the manipulator design has a modular platform that allows for different end effectors to be mounted on it. The two initial end effectors will accommodate biopsy guns and brachytherapy needles. Both require an

insertion phase; the former requires activating a single-acting button to engage the device and a safety lock. The latter requires an additional controlled linear motion to accommodate the cannula retraction to release the brachytherapy seeds($DOF\#7$). Rotation of the needle about its axis may be implemented to either "drill" the needle in to limit deflect, or to steer the needle using bevel steering techniques such as those described by Webster et al. in [29]. Sterility has been taken into consideration for the design of the end effectors. In particular, the portions of the manipulator and leg rest that come in direct contact with the patient or needle will be removable and made of materials that are suitable for sterilization. The remainder of the robot will be draped. Alternatively, the entire leg rest with the robot will be covered in a sterile drape, thus completely isolating the robot from the patient except for the needle.

3.2 Mechanism Design

The mechanism design is particulary important since there are very confined spaces and the robot is constructed without the use of metallic links. The design was developed such that the kinematics can be simplified, control can be made less complex, motions may be decoupled, actuators can be aligned appropriately and system rigidity can be increased. Based upon analysis of the workspace and the application, the following additional design requirements have been adopted:

1. Linear base motion should be able to be decoupled from the rotations since the majority of procedures will not require the two rotational DOF.

2. Actuator motion should be in the axial direction (aligned with the scanner's axis) to maintain a compact profile.

3. Extension in both the vertical and horizontal planes should be telescopic to minimize the working envelope.

The four primary base degrees of freedom ($DOF\#2$-5 in Table 1) are broken into two decoupled 2-DOF planar motions. The planar bar mechanisms allow for high rigidity. Other power transfer techniques evaluated include cables, pulleys, gears, linear slides, leadscrews, etc.; however, these were avoided in an attempt to design a very reliable, robust, compact, and rigid system.

Motion in the vertical plane includes $100mm$ of vertical travel, and up to 15° of elevation angle. This is achieved using a modified version of a scissor lift mechanism. Coupling two such mechanisms, as shown in Fig. 3, permits the two desired DOF. Stability is increased by using a pair of such mechanisms in the rear. For purely prismatic, both slides move in unison; angulation (θ) is generated by relative motions. To aid in decoupling, the actuator for the rear slide can be fixed to the carriage of the primary motion linear drive, thus allowing one actuator to be locked when angulation is not required. As shown in Fig. 3, the push rods for the front and rear motions are coupled together to provide only prismatic motion in the initial prototype.

Motion in the horizontal plane is accomplished with a second planar bar mechanism. This motion is achieved by coupling two straight line motion mechanisms as shown in Fig. 4, generally referred to as Scott-Russell mechanisms [30]. By combining two such straight-line motions, both linear and rotational motions can be realized in the horizontal plane; this mechanism allows for bilateral motion with respect to the nominal center position. Actuation is provided by custom, MR-compatible pneumatic cylinders that are oriented in the axial direction. Fig. 4 shows the mechanism with only translation is available; this is accomplished by linking the front and rear

mechanisms with a connecting bar. It is straightforward to add the rotational motion for future designs by replacing the rigid connecting bar (L_C) with another pneumatic cylinder; translational motion remains decoupled when rotation is not used by ensuring that the cylinder in the connecting bar remains locked. For ease of manufacturing, the first version of the system is made primarily out of acrylic. In future design iterations, the links will be made out of high strength, dimensionally stable, highly electrically insulating and sterilizable plastic (e.g. Ultem or PEEK).

3.3 Actuator Design

The MRI environment places severe restrictions on the choice of sensors and actuators. Many mechatronic systems use electro-dynamic actuation, however, the very nature of an electric motor precludes its use in high-field magnetic environments. Therefore, it is necessary to: 1) use actuators that are compatible with the MR environment, or 2) to use a transmission to mechanically couple the manipulator in close proximity to the scanner to standard actuators situated outside the high field. MR compatible actuators such as piezoceramic motors have been evaluated in [16, 24, 25]; however, these are prone to introducing noise into MR imaging and therefore negatively impacting image quality. The latter can take the form of flexible driveshafts [18], push-pull cables, or hydraulic (or pneumatic) couplings [23].

To maintain close proximity of the actuators to the robot, alternatives to electric motors include hydraulic and pneumatic actuators. Hydraulic actuators offer the advantages of high stiffness and near-incompressible flow at the expense of speed/bandwidth, more difficult fluid connections, and the potential for leaks. Portability of the system and ease of connections contradicts the closed-system nature of hydraulic actuators. Pneumatic actuators offer relatively high speed, large avail-

ability of components and readily available compressed air supply at the expense of decreased rigidity and less straightforward control due to the compressibility of air and the relatively large non-linear friction forces in the cylinder. Accurate servo control of pneumatic actuators using sliding mode control (SMC) with submillimeter tracking accuracy and $0.01mm$ SSE has been demonstrated in [31]. Pneumatics were the actuator of choice for this robot.

Although pneumatic actuation seems ideal for MRI, most standard pneumatic cylinders are not suitable for use in MRI. Custom MR compatible pneumatic cylinders have been developed for use with this robot. The cylinders are based upon Airpel $9.3mm$ bore cylinders [1]. These cylinders were chosen because the cylinder bore is made of glass and the piston and seals are made of graphite. This design has two main benefits; the primary components are suitable for MRI and they inherently have very low friction (as low as $1g$). In collaboration with the manufacturer, we developed the cylinders shown in Fig. 5 that are entirely nonmetallic except for the brass shaft. The cylinders can handle up to $100psi$ $(6.9bar)$ and therefore can apply forces up to $46.8N$. In addition to precisely moving the robot, it is important to be able to lock it in position to provide a stable needle insertion platform. Pneumatically operated, MR compatible brakes have been developed for this purpose. The brakes are compact units that attach to the ends of the previously described cylinders as shown in Fig. 4 and clamp down on the rod. The design is such that the fail-safe state is locked and applied air pressure releases a spring-loaded collet to enable motion. The brakes are disabled when the axis is being aligned, and applied when the needle is to be inserted or an emergency situation arises.

There are three basic valve types typically used for servo control of a cylinder: 1) High-

[1] Airpel E9 Anti-stiction Air Cylinder - http://www.airpel.com

bandwidth on-off valves, 2) Proportional flow spool valves, and 3) Proportional pressure regulator valves. Proportional pressure regulators were the valve of choice for this robot because they allow for direct control of the pressure, thus the force, on the robot. This is an advantage because it aids in controller design and also has the inherent safety of being able to limit applied pressure to a prescribed amount.

Pneumatic valves are typically operated directly by a solenoid coil or indirectly by a small pilot valve that is actuated by a solenoid coil. Unfortunately, as with electric motors, the very nature of a solenoid coil is a contraindication for its use in an MR environment. With pneumatic control, it is essential to limit the distance from the valve to the cylinder on the robot; thus it is important to use valves that are safe and effective in the MR environment. By placing the controller in the scanner room near the foot of the bed, air tubing lengths can be reduced to $5m$. The robot controller uses piezoelectrically actuated proportional pressure valves[2] that do not use traditional solenoid coil, thus permitting their use near MRI. A pair of these valves provide a differential pressure of $\pm 100psi$ on the cylinder piston for each actuated axis. A further benefit of piezoelectrically actuated valves is the rapid response time ($4ms$). Thus, by using piezoelectric valves the robot's bandwidth can be increased significantly by limiting tubing lengths and increasing controller update rate.

3.4 Position Sensing

Standard methods of position sensing that are generally suitable for pneumatic cylinders include: linear potentiometers, linear variable differential transformers (LVDT), capacitive sensors, ultra-

[2]Hoerbiger-Origa PRE-U piezo valve - http://www.hoerbigeroriga.com

sonic sensors, magnetic sensors, laser sensors, optical encoders, and cameras (machine vision). Most of these sensing modalities are not practical for use in an MR environment. However, there are two methods that do appear to have potential: 1) linear optical encoders and 2) direct MRI image guidance.

3.4.1 Joint Encoding

Standard optical encoders[3] have been thoroughly tested in a 3T MRI scanner for functionality and induced effects in the form of imaging artifacts as described in [27]. The encoders have been incorporated into the robot and have performed without any stray or missed counts; the imaging artifact is confined locally to within 2-5cm from the encoder. This is sufficient because the robot is designed to distance the sensors from the prostate imaging volume.

3.4.2 Registration to MR Imaging

Direct MRI-based image guidance shows great promise for high-level control, safety and verification. However, the refresh rate and resolution is not sufficient for use in low-level servo control of a robot joint. Practical methods of robot tracking are discussed in [18].

Inherently, the robot system has two different coordinate systems: 1) the image coordinate system for the imaging, planning and verification, and 2) the robot coordinate system based on the encoders for servo control of the robot joint described in Section 3.4. The interpretation of positional information between these two coordinate systems is crucial for the targeting accuracy. To achieve dynamic global registration between the robot and image coordinates a Z-shaped passive tracking fiducial is attached on the robot base. The rigid structure of the fiducial frame is made up

[3]EM1-1250 and E5D-1250 encoder modules with PC5 differential line driver - US Digital, Vancouver, Washington

of seven rigid glass tubes with $3mm$ inner diameters that are filled with contrast agent extracted from commercially available MRI fiducials[4]. The rods are placed on three faces of a $60mm$ cube as shown in Fig. 5, and any arbitrary MR image slicing through rods provides the full 6 DOF pose of the frame, and hence the robot, with respect to the scanner. The accuracy of localization using this frame is better than $0.2mm$ and 0.4°; a detailed description of the tracking techniques and accuracy analysis as described in [32].

Thus, by locating the fiducial attached to the robot, the transformation between image coordinate (where planning is performed) and the robot coordinate is known. Once the transformation is known, the end effector location is calculated from the kinematics and encoder positions and transformed to the representation in the image coordinate system. Alternatively, the encoder positions corresponding to targets are calculated from the inverse-kinematics based on the target points specified on the image and transformed to the representation in the robot coordinate.

3.5 Robot Controller Hardware

MRI is very sensitive to electrical signals passing in and out of the scanner room. Electrical signals passing through the patch panel or wave guide can act as antennas, bringing stray RF noise into the scanner room. For that reason, and to minimize the distance between the valves and the robot, the robot controller is placed inside of the scanner room with no external electrical connections. The controller comprises an EMI shielded enclosure that sits at the foot of the scanner bed as shown in Fig. 7; the controller has proved to be able to operate $3m$ from the edge of the scanner bore. Inside of the enclosure is an embedded computer with analog I/O for interfacing with valves and

[4]MR Spots - Beekley, Bristol, CT

pressure sensors and an FPGA module for interfacing with joint encoders (See Fig. 6). Also in the enclosure are the piezoelectric servo valves, piezoelectric brake valves and pressure sensors. The distance between the servo valves and the robot is minimized to less than $5m$, thus maximizing the bandwidth of the pneumatic actuators. The expected bandwidth is 100Hz. Control software on the embedded PC, provides for low level joint control and an interface to interactive scripting and higher level trajectory planning. Low-level control software is implemented on the embedded computer inside the robot controller enclosure inside the scanner room. The computer runs Linux using the Real Time Application Interface (RTAI)[5] kernel extension to allow for the accurate clock necessary for PC-based servo control.

Pneumatic connections from the robot interface to the manipulator that is sitting on the bed in the scanner bore are simplified with a multi-port pneumatic connector and bundled air tubing that can accommodate up to 10 connections in a single plug. Encoder connections to the robot are made using a single standard 68-conductor shielded, twisted pair cable that mates to the robot axes through a custom circuit board on the robot with individual connectors per axis as in Fig. 7. Communication between the low-level control PC and the planning and control workstation sitting in the MR console room is through a fiber optic Ethernet connection. No electrical connections pass out of the scanner room, thus significantly limiting the MR imaging interference.

3.6 Interface Software

3D Slicer surgical navigation software[6] serves as a user interface with the robot. The navigation software is running on a Linux-based workstation in the scanner's console room. A customized

[5]RTAI - http://www.rtai.org
[6]3D Slicer - http://www.slicer.org

graphical user interface (GUI) specially designed for the prostate intervention with the robot is described in [33]. The interface allows smooth operation of the system throughout the clinical workflow including registration, planning, targeting, monitoring and verification (Fig. 9). The workstation is connected to the robot and the scanner's console via Ethernet. An open-source device connection and communication tool originally developed for virtual reality research [34] is used to exchange various types of data such as control commands, positional data, and images among the components. The data flow is defined by XML files and flexibly configurable without rebuilding the software. Fig. 8 shows the configuration used in the system.

In the planning phase, pre-operative images are retrieved from a DICOM server and loaded into the navigation software. Target points for the needle insertion are selected according to the pre-operative imaging, and the coordinates of the determined target points are selected in the planning GUI. Once the patient and the robot are placed in the MRI scanner, a 2D image of the fiducial frame is acquired and passed to the navigation software to calculate the 6-DOF pose of the robot base for the robot-image registration as described in Section 3.4.2. The position and orientation of the robot base is sent through the network from the navigation software to the robot controller. After the registration phase, the robot accepts target coordinates represented in the image (patient) coordinate system.

During the procedure, a target and an entry point are chosen on the navigation software, and the robot is sent the coordinates and aligns the needle guide appropriately. In the current system, the needle is inserted manually while the needle position is monitored by an encoded needle guide and displayed in real-time on the display. Needle advancement in the tissue is visualized on the

navigation software in two complementary ways: 1) a 3D view of needle model combined with pre-operative 3D image resliced in planes intersecting the needle axis, and 2) 2D real-time MR images acquired from the planes along or perpendicular to the needle path and continuously obtained from the scanner. The former provides a high refresh rate, typically ($10Hz$), allowing a clinician to manipulate the needle interactively, while the latter provides the changing shape or position of the target lesion with relatively slower rate depending on the imaging speed, typically 0.5 frames per second.

The interface software enables "closed-loop" needle guidance, where the action made by the robot is captured by the MR imaging, and immediately fed back to a physician to aid their decision for the next action. The reason for keeping a human in the loop is to increase the safety of the needle insertion, and to allow for the live MR images to monitor progress. Fig. 9 shows the planning software with an MR image of the phantom loaded and real-time feedback of the robot position is used to generate the needle axis model.

4 Results

The first iteration of the needle placement robot has been constructed and is operational. All mechanical, electrical, communications, and software issues have been resolved. The current state of the manipulator is two actuated DOF (vertical and horizontal) with an encoded passive needle insertion stage as shown in Fig. 5. Evaluation of the robot is in three distinct phase: 1) evaluation of the MR compatibility of the robot, 2) evaluation of the workspace and workflow, and 3) evaluation of the localization and placement accuracy.

4.1 MR Compatibility

MR compatibility includes three elements: 1) safety, 2) preserving image quality, and 3) maintaining functionality. Safety issues such as RF heating are minimized by isolating the robot from the patient, avoiding wire coils, and avoiding resonances in components of the robot; ferrous materials are completely avoided to prevent the chance of a projectile. Image quality is maintained by again avoiding ferromagnetic materials, limiting conductive materials near the imaging site, and avoiding RF sources that can interfere with the field homogeneity and sensed RF signals. Pneumatic actuation and optical sensing, as described in Section 3, preserve full functionality of the robot in the scanner during imaging. The MR compatibility of the system is thoroughly evaluated in [27].

Compatibility was evaluated on a 3T Philips Achieva scanner. A $10cm$, fluid-filled spherical MR phantom was placed in the isocenter and the robot placed such that the tip was at a distance of $120mm$ from the center of the phantom (a representative depth from perineum to prostate) as shown in Fig. 11 (left). The phantom was imaged using three standard prostate imaging protocols: 1) **T2W TSE**: T2 weighted turbo spin echo (28cm FOV, 3mm slice, TE=90ms, TR=5600ms, 2) **T1W FFE**: T1 weighted fast field gradient echo (28cm FOV, 3mm slice, TE=2.3ms, TR=264ms) and 3) **TFE (FGRE)**: "Real time" turbo field gradient echo (28cm FOV, 3mm slice, TE=10ms, TR=26ms). The following imaging series were taken in each of the following configurations: 1) Phantom only (baseline), 2) Controller in room and powered, 3) Robot placed in scanner bore, 4) Robot electrically connected to controller and 5) Robot moving during imaging (only with T1W imaging).

The degradation of signal to noise ratio (SNR) was used as the measure of negative effects

on image quality. SNR was defined as the mean signal in a $25mm$ square at the center of the homogeneous sphere divided by the standard deviation of the signal in that same region. The SNR of the magnitude images was normalized by the value for the baseline image; thus limiting any bias in choice of calculation technique or location. Normalized SNR was evaluated at seven $3mm$ thick slices (representing a $25mm$ cube) at the center of the sphere for each of the three imaging sequences. The points in the graph in Fig. 12 show the SNR for each of the slices for each sequence at each configuration, and the lines represent the average SNR in the $25mm$ cube.

When the robot was operational, the reduction in SNR of the cube at the phantom's center for these pulse sequences was 5.5% for **T1W FFE**, 4.2% for **T2W TSE** and 1.1% for **TFE (FGRE)**. Further qualitative means of evaluating the effect of the robot on image quality are obtained by examining prostate images taken both with and without the presence of the robot. Fig. 13 (right) shows images of the prostate of a volunteer placed in the scanner bore on the leg rest. With the robot operational, there is no visually identifiable loss in image quality of the prostate.

4.2 System Integration and Workflow

In the traditional workflow, the clinician is scrubbed in and remains inside the scanner room with the patient for the entirety of the procedure. Therefore, it is important to be able to control the robot from within the scanner room. Before the procedure begins, target locations and needle trajectories are selected on the planning workstation using pre-procedural images (with additional information from fused pre-operative, multi-modality imaging). These target locations can be visualized on an MR-compatible display present inside the scanner room, selected intraoperatively and updated as necessary. Due to the ability to track the robot end effector, the MR scan plane can be controlled to

automatically provide images along the needle axis. Therefore, as the robot aligns the needle axis with the plan, alignment is confirmed with MR images taken along the needle axis showing both the needle and the target. The calculated robot position with respect to the target is also displayed on the planning workstation. The needle is inserted manually along the passive, encoded needle guide with real-time (two second capture time) images being displayed as it is inserted and the position updated on the display.

To evaluate the overall layout and workflow, the robot was placed in the bore inside of the leg rest with a volunteer as shown in Fig. 13 (left). Round flex receiver coils were used for this trial; endorectal coils can be used for clinical case to obtain optimal image quality. There was adequate room for a patient and the robot was able to maintain its necessary workspace. Further studies of this are underway where volunteers are imaged on the leg rest in the appropriate semi-lithotomy position and the prostate and anatomical constraints are analyzed.

Co-registration of the robot to the scanner was performed using the tracking fiducial described in Section /refsection:control that is shown in Fig. 5. Images of the robot's tracking fiducial provide the location of the robot base in the scanner's coordinate system with an RMS accuracy of $0.14mm$ and $0.37°$. The joint encoders on the robot allow the end effector position and orientation to be determined with respect to the robot. The end effector localization accuracy is nonlinear due to the mechanism design; based on encoder resolution, the worst case resolution for link localization for the horizontal and vertical motions is $0.01mm$ and $0.1mm$ respectively. The overall accuracy of needle tip localization with respect to the MR images is better than $0.25mm$ and $0.5°$.

4.3 Accuracy

Accuracy assessment is broken into two parts: localization and placement. These two must be distinguished, especially in many medical applications. In prostate biopsy, it is essential to know exactly where a biopsy comes from in order to be able to form a treatment plan if cancer is located. In brachytherapy treatment, radioactive seed placement plans must be made to avoid cold spots where irradiation is insufficient; by knowing where seeds are placed, the dosimetry and treatment plan can be interactively updated. Based on encoder resolution, localization accuracy of the robot is better than $0.1mm$ in all directions. Positioning accuracy is dependent on the servo pneumatic control system. With the controller hardware complete and a preliminary controller based upon standard PID techniques in place, the robot can be positioned within about $5mm$. Development and refinement of novel pneumatic control architecture is underway, and the goal is for the target positioning accuracy to approach the resolution of the encoders. Experiments with sliding mode control algorithms that are more robust to the high friction of the mechanism show great promise, and we intend to achieve $0.1mm$ positioning accuracy per axis.

5 Discussion and Future Work

We have developed an MRI-compatible manipulator and the support system architecture that can be used for needle placement in the prostate for biopsy and brachytherapy procedures. The robot has been designed such that it will operate in the confined space between the patient's legs inside a leg rest/tunnel in a high-field, closed bore MRI scanners. Unlike any other attempts at transperineal robotic prostate interventions, the patient is in the semi-lithotomy position. This affords several

benefits: 1) pre-operative imaging corresponds directly to the intra-procedural images, 2) patient and organ motion is limited and 3) the workflow of the conventional TRUS procedure can be preserved. The configuration allows the use of diagnostic MRI scanners in interventional procedures; there is no need for open or large bore scanners that often are difficult to come by and sacrifice image quality.

Attaining an acceptable level of MR compatibility required significant experimental evaluation. Several types of actuators including were evaluated including piezoelectric motors and several pneumatic cylinders and valves. The author's experiences with piezoelectric motors were not as positive as reported elsewhere in the literature; although high quality images could be attained with the system in the room, noticeable noise was present when the motors were running during imaging. This prompted the investigation of pneumatic actuators. Pneumatic actuators have great potential for MRI compatible mechatronic systems. Since no electronics are required, they are fundamentally compatible with the MR environment. However, there are several obstacles to overcome. These include 1) material compatibility which was overcome with custom cylinders made of glass cylinders and graphite pistons, 2) lack of stiffness or instability which was overcome with the development of a pneumatic brake that locks the cylinder's rod during needle insertion, and 3) difficult control which was ameliorated by using high-speed valves and shortening pneumatic hose lengths by designing and MRI compatible controller. Pneumatic actuation seems to be an ideal solution for this robotic system, and it allows the robot to meet all of the design requirements set forth in Section 2. Further, MR compatibility of the system including the robot and controller is excellent with no more that a 5% loss in average SNR with the robot operational.

The system has been evaluated in several ways. First, the physical configuration of the robot and controller seems ideal for this procedure. The MR compatibility has shown to be sufficient for anatomical imaging using traditional prostate imaging sequences. Communications between all of the elements including the robot, the low level controller, the planning workstation and the MR scanner real-time imaging interface are in place. Initial phantom studies validated the workflow and the ability to accurately localize the robot and target a lesion.

The primary elements of the system are now in place. Current work focusses on refinement of the control system and interface software. The next phase of this work focusses on generating clinical-grade system and preparing for Phase-1 clinical trials. The initial application will be prostate biopsy, followed later by brachytherapy seed placement. With the addition of the two rotational DOF, the design of the manipulator allows for treatment of patients that may have otherwise been denied such treatment because of contraindications such as significant pubic arch interference. The robot, controller and/or system architecture are generally applicable to other MR robotic applications. We intend to deploy a platform not only for prostate biopsy and brachytherapy, but also for injections, thermal ablation, and optical sensing modalities under MR image guidance.

Acknowledgements

This work was supported by NSF EEC-97-31478, NIH BRP RO1-CA111288-01, NIH/NIBIB R01-EB002963-01, NIH U41-RR019703, and CDMRP PCRP Fellowship W81XWH-07-1-0171.

References

[1] A. Jemal, “Cancer statistics, 2004,” in *CA Cancer J Clin*, vol. 54(8), 2004.

[2] J. C. Blasko and et al., "Brachytherapy for carcinoma of the prostate: techniques, patient selection, and clinical outcomes," in *Semin Radiat Oncol*, vol. 12(1), pp. 81–94, 2002.

[3] M. R. Cooperberg and et al., "The changing face of low-risk prostate cancer: trends in clinical presentation and primary management," in *J Clin Oncol*, vol. 22(11), pp. 2141–9, 2004.

[4] J. C. Presti Jr., "Prostate cancer: assessment of risk using digital rectal examination, tumor grade, prostate-specific antigen, and systematic biopsy," in *Radiol Clin North Am*, vol. 38(1), pp. 49–58, 2000.

[5] M. K. Terris and et al., "Comparison of mid-lobe versus lateral systematic sextant biopsies in detection of prostate cancer," in *Urol Int*, vol. 59, pp. 239–242, 1997.

[6] D. W. Keetch and et al., "Prostate specific antigen density versus prostate specific antigen slope as predictors of prostate cancer in men with initially negative prostatic biopsies," in *J Urol*, vol. 156(2 Pt 1), pp. 428–31, 1996.

[7] A. V. D'Amico, R. Cormack, C. M. Tempany, S. Kumar, G. Topulos, H. M. Kooy, and C. N. Coleman, "Real-time magnetic resonance image-guided interstitial brachytherapy in the treatment of select patients with clinically localized prostate cancer," in *International Journal of Radiation Oncology*, vol. 42, pp. 507–515, Oct. 1998.

[8] A. V. D'Amico, C. M. Tempany, R. Cormack, N. Hata, and et al., "Transperineal magnetic resonance image guided prostate biopsy," in *J Urol*, vol. 164(2), pp. 385–7, 2000.

[9] S. Zangos, K. Eichler, K. Engelmann, M. Ahmed, S. Dettmer, C. Herzog, W. Pegios, A. Wetter, T. Lehnert, M. G. Mack, and T. J. Vogl, "MR-guided transgluteal biopsies with an open

low-field system in patients with clinically suspected prostate cancer: technique and preliminary results," in *Eur Radiol*, vol. 15(1), pp. 174–82, 2005.

[10] R. C. Susil, K. Camphausen, P. Choyke, E. R. McVeigh, G. S. Gustafson, H. Ning, R. W. Miller, E. Atalar, C. N. Coleman, and C. Ménard, "System for prostate brachytherapy and biopsy in a standard 1.5 T MRI scanner," in *Magnetic Resonance in Medicine*, vol. 52, pp. 683–6873, 2004.

[11] D. Beyersdorff, A. Winkel, B. Hamm, and et al., "MRI-guided prostate biopsy with a closed MR unit at 1.5 T," in *Radiology*, vol. 234, pp. 576–581, 2005.

[12] N. V. Tsekos, A. Khanicheh, E. Christoforou, and C. Mavroidis, "Magnetic ResonanceCompatible Robotic and Mechatronics Systems for Image-Guided Interventions and Rehabilitation: A Review Study," in *Annual Review of Biomedical Engineering*, vol. 9, pp. 351–387, Aug. 2007.

[13] K. Masamune, E. Kobayashi, Y. Masutani, M. Suzuki, T. Dohi, H. Iseki, and K. Takakura, "Development of an MRI-compatible needle insertion manipulator for stereotactic neurosurgery," in *J Image Guid Surg*, vol. 1(4), pp. 242–8, 1995.

[14] A. Felden, J. Vagner, A. Hinz, H. Fischer, S. O. Pfleiderer, J. R. Reichenbach, and W. A. Kaiser, "ROBITOM-robot for biopsy and therapy of the mamma," in *Biomed Tech (Berl)*, vol. 47 Suppl 1 Pt 1, pp. 2–5, 2002.

[15] E. Hempel, H. Fischer, L. Gumb, and et al., "An MRI-compatible surgical robot for precise radiological interventions," in *CAS*, pp. 180–191, Apr. 2003.

[16] K. Chinzei, N. Hata, F. A. Jolesz, and R. Kikinis, "MR compatible surgical assist robot: system integration and preliminary feasibility study," in *MICCAI*, vol. 1935, pp. 921–933, Oct. 2000.

[17] S. P. DiMaio, S. Pieper, K. Chinzei, G. Fichtinger, C. Tempany, and R. Kikinis, "Robot assisted percutaneous intervention in open-MRI," in *MRI Symp*, p. 155, 2004.

[18] A. Krieger, R. C. Susil, C. Menard, J. A. Coleman, G. Fichtinger, E. Atalar, and L. L. Whitcomb, "Design of a novel MRI compatible manipulator for image guided prostate interventions," in *IEEE TBME*, vol. 52, pp. 306–313, Feb. 2005.

[19] D. Stoianovici, A. Patriciu, D. Petrisor, D. Mazilu, and L. Kavoussi, "A New Type of Motor: Pneumatic Step Motor," in *IEEE/ASME Trans Mechatronics*, vol. 12(1), pp. 98–106, Feb. 2007.

[20] H. Elhawary, A. Zivanovic, M. Rea, Z. T. H. Tse, D. McRobbie, I. Young, B. D. M. Paley, and M. Lamprth, "A MR Compatible Mechatronic System to Facilitate Magic Angle Experiments in Vivo," in *MICCAI*, pp. 604–611, Nov. 2007.

[21] D. N. Zaman, T. Suzuki, H. Liao, E. Kobayashi, Y. Jimbo, and I. Sakuma, "Development and Evaluation of a Novel Actuator using MR Magnetic Field," in *IEEE IROS*, pp. 1184–1189, Oct. 2007.

[22] E. Taillant, J. Avila-Vilchis, C. Allegrini, I. Bricault, and P. Cinquin, "CT and MR Compatible Light Puncture Robot: Architectural Design and First Experiments," in *MICCAI*, vol. 3217, pp. 145–152, 2004.

[23] R. Gassert, R. Moser, , E. Burdet, and H. Bleuler, "MRI/fMRI-Compatible Robotic System With Force Feedback for Interaction With Human Motion," in *T. Mech.*, vol. 11(2), pp. 216–24, Apr. 2006.

[24] T. Suzuki, H. Liao, E. Kobayashi, and I. Sakuma, "Ultrasonic motor driving method for EMI-free image in MR image-guided surgical robotic system," in *IEEE IROS*, pp. 522–527, Oct. 2007.

[25] H. Elhawary and et al, "The Feasibility of MR-Image Guided Prostate Biopsy Using Piezoceramic Motors Inside or Near to the Magnet Isocentre," in *MICCAI*, vol. 4190, pp. 519–526, 2006.

[26] D. Stoianovici, D. Song, D. Petrisor, D. Ursu, D. Mazilu, M. Mutener, M. Schar, and A. Patriciu, "'MRI Stealth" robot for prostate interventions," in *Minimally Invasive Therapy and Allied Technologies*, vol. 16(4), pp. 241–248, July 2007.

[27] G. S. Fischer, S. P. DiMaio, I. Iordachita, and G. Fichtinger, "Development of a Robotic Assistant for Needle-Based Transperineal Prostate Interventions in MRI," in *MICCAI*, Nov. 2007.

[28] K. Wallner, J. Blasko, and M. Dattoli, *Prostate Brachytherapy Made Complicated, 2nd Ed.* SmartMedicine Press, 2001.

[29] R. J. Webster III, J. S. Kim, N. J. Cowan, G. S. Chirikjian, and A. M. Okamura, "Nonholonomic Modeling of Needle Steering," in *International Journal of Robotics Research*, vol. 25(2), pp. 509–525, May 2006.

[30] P. Schwamb and A. L. Merrill, *Elements of Mechanism*. 1905.

[31] G. M. Bone and S. Ning, "Experimental Comparison of Position Tracking Control Algorithms for Pneumatic Cylinder Actuators," in *IEEE/ASME Transactions on Mechatronics*, vol. 12, pp. 557–561, Oct. 2007.

[32] S. P. DiMaio, E. Samset, G. S. Fischer, I. Iordachita, G. Fichtinger, F. Jolesz, and C. Tempany, "Dynamic MRI Scan Plane Control for Passive Tracking of Instruments and Devices," in *MICCAI*, Nov. 2007.

[33] P. Mewes, J. Tokuda, S. P. DiMaio, G. S. Fischer, C. Csoma, D. G. Gobi, C. Tempany, G. Fichtinger, and N. Hata, "An Integrated MRI and Robot Control Software System for an MR-compatible Robot in Prostate Intervention," in *IEEE ICRA (in review)*, May 2008.

[34] J. V. Spiczak, E. Samset, S. P. Dimaio, G. Reitmayr, D. Schmalstieg, C. Burghart, and R. Kikinis, "Device connectivity for image-guided medical applications," in *Stud Health Technol Inform*, pp. 125:482–4, 2007.

Figures

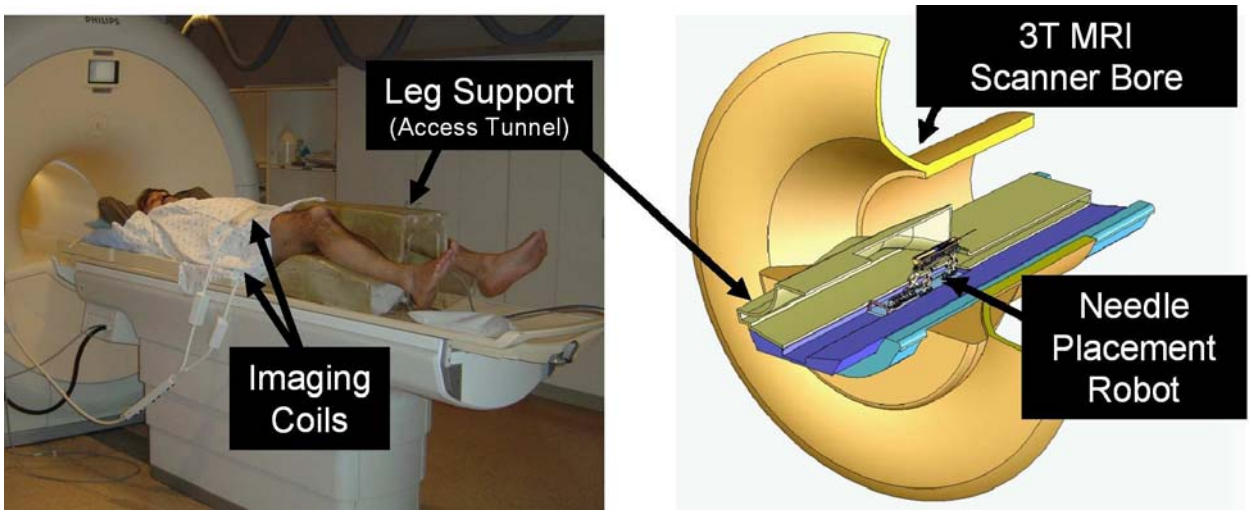

Figure 1: Proposed patient positioning in the semi-lithotomy position on the leg support (left) and robot position within the access tunnel (right). Access to the prostate is made through the perineal wall which rests against the superior surface of the leg rest.

Table 1: Kinematic Specifications

	Degree of Freedom	Motion	Requirements
1)	Gross Axial Position	1m	Manual with repeatable stop
2)	Vertical Motion	0-100mm	Precise servo control
3)	Elevation Angle	$+15°, -0°$	Precise servo control
4)	Horizontal Motion	$\pm$50mm	Precise servo control
5)	Azimuth Angle	$\pm 15°$	Precise servo control
6)	Needle Insertion	150mm	Manual or Automated
7)	Canula Retraction or Biopsy Gun Firing	60mm	Manual or Automated
8)	Needle Rotation	360°	Manual or Automated

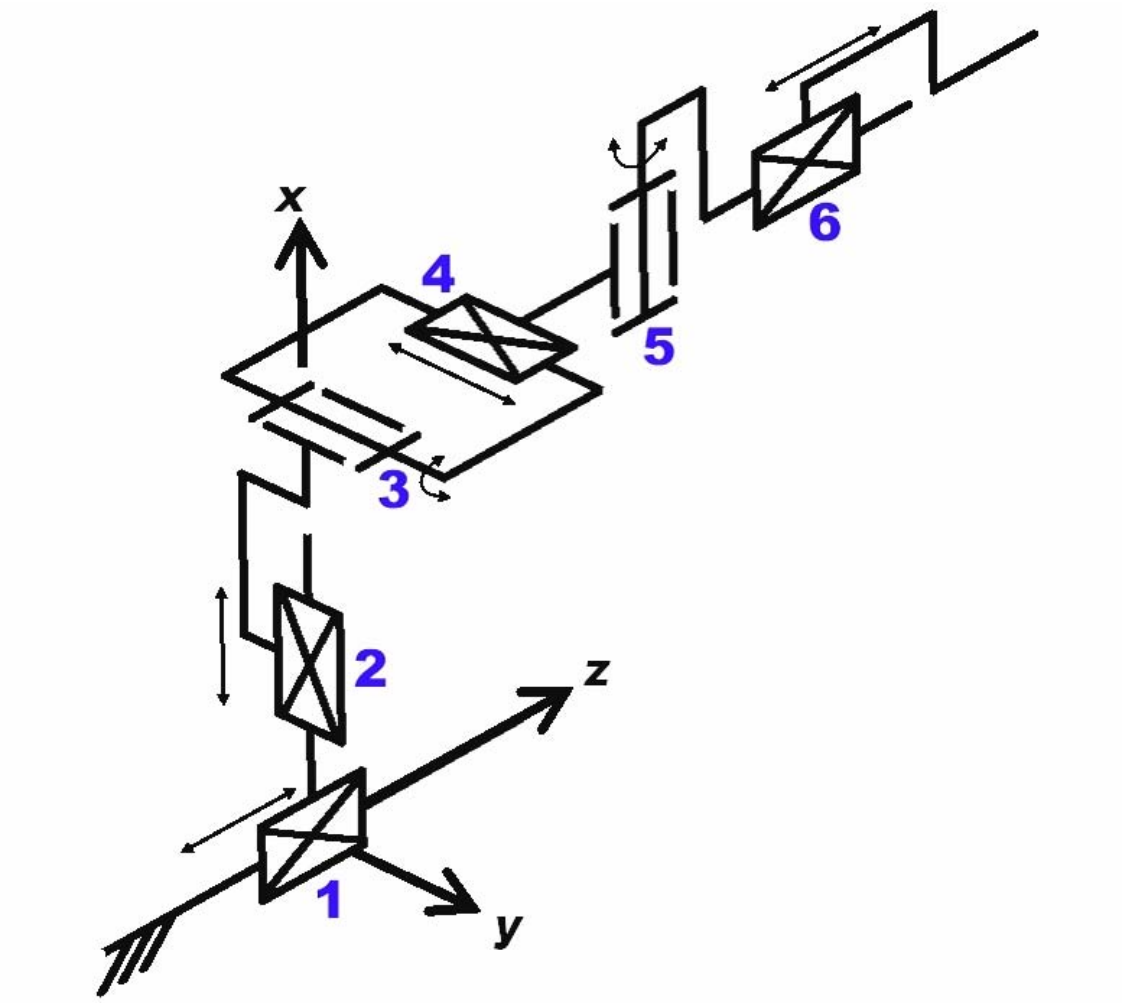

Figure 2: The equivalent kinematic diagram of the robot; six degrees of freedom are required for needle insertion procedures with this manipulator. Additional application-specific end effectors may be added to provide additional DOF.

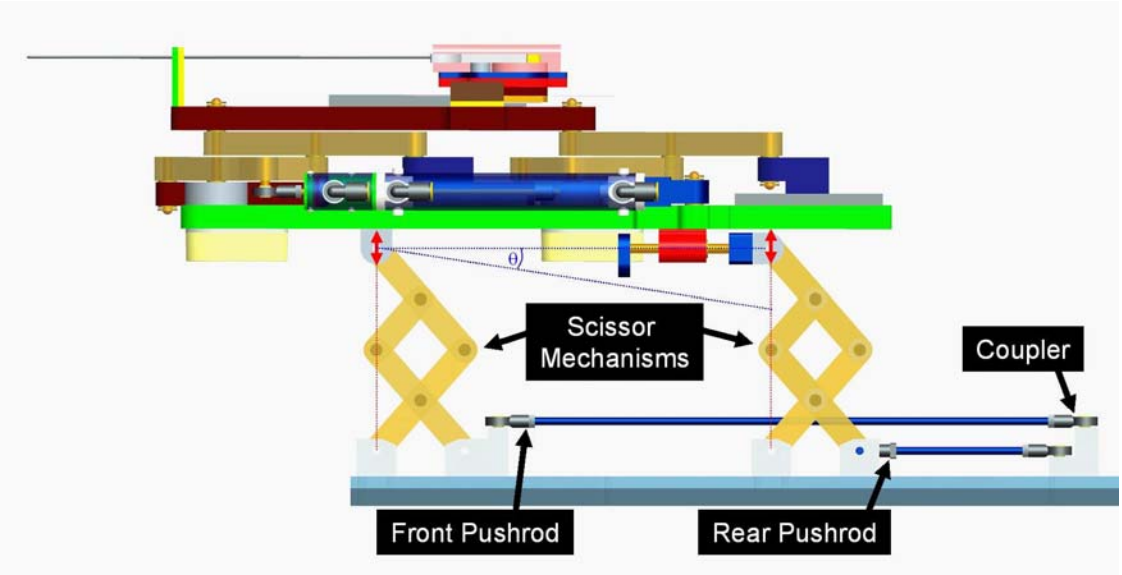

Figure 3: This mechanism provides for motion in the vertical plane. Coupling the forward and rear motion provides for vertical travel, independently moving the rear provides for elevation angle (θ) adjustment.

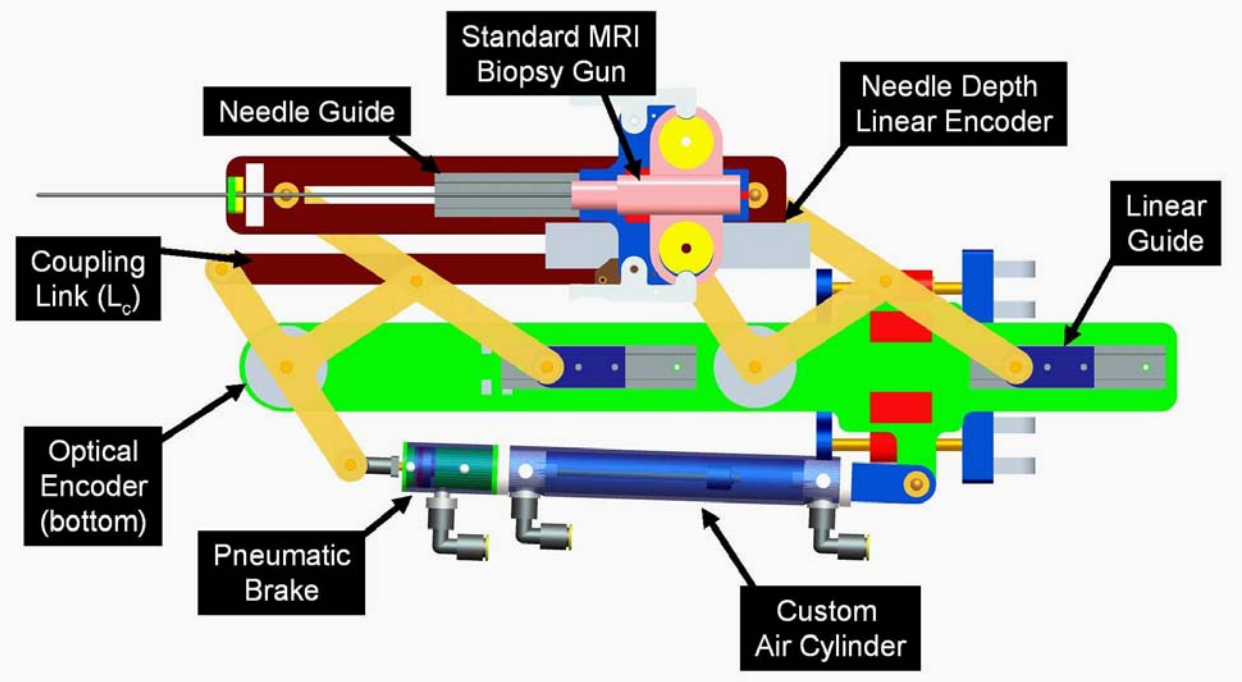

Figure 4: This mechanism provides for motion in the horizontal plane. Only prismatic motion is available in the design shown; rotation can be enabled by actuating rear motion independently by replacing coupling link (L_C) with a second cylinder. The encoded needle guide senses the depth during manual needle insertion. The modular needle guide can be replaced with different end effectors for other procedures.

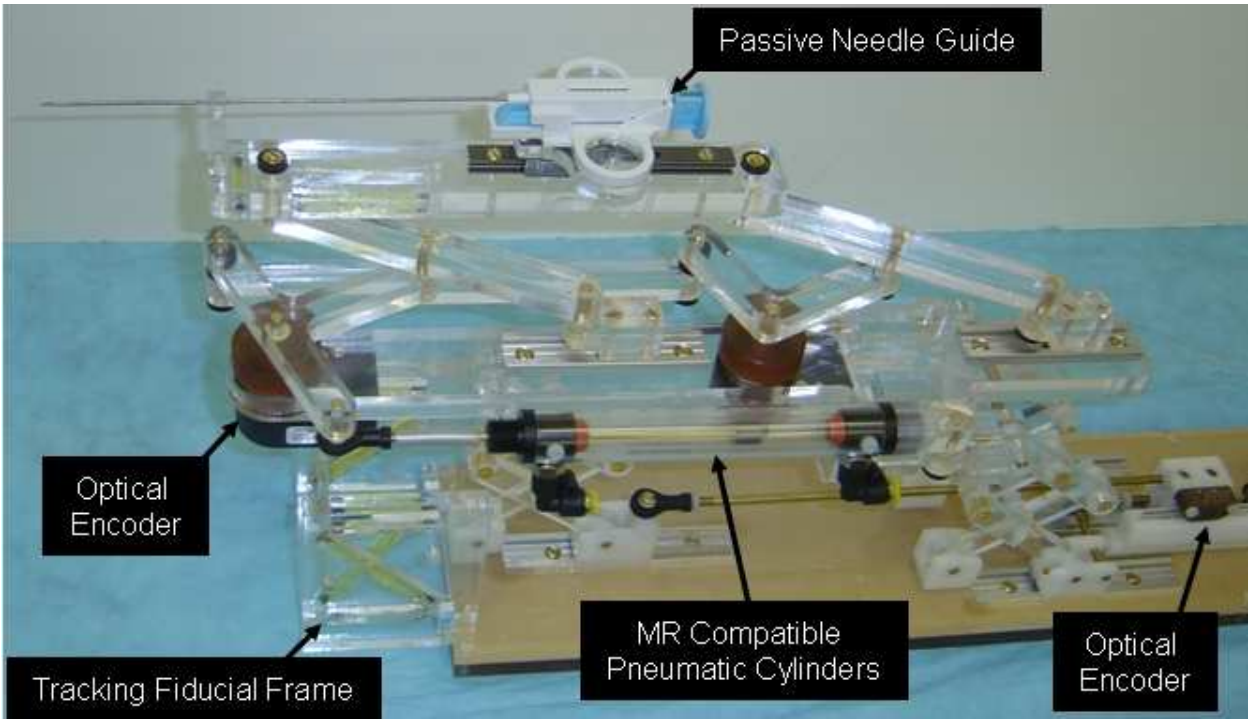

Figure 5: The robotic needle placement mechanism with two active DOF and one passive, encoded needle insertion. Dynamic global registration is achieved with the attached tracking fiducial.

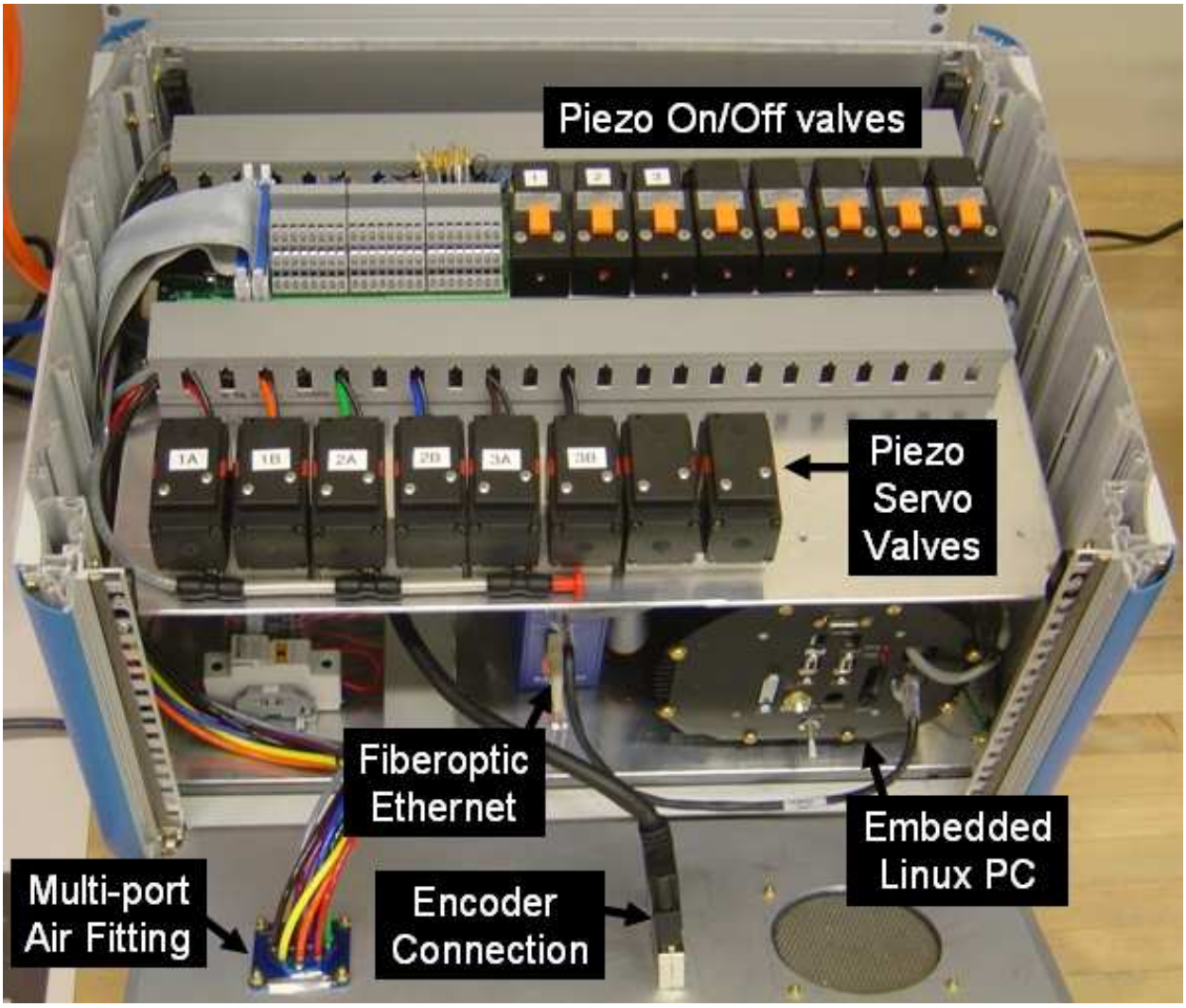

Figure 6: The controller contains the embedded Linux PC providing low-level control, the piezo-electric valves and the fiber optic ethernet converter. The EMI shielded enclosure is placed inside the scanner room near the root of the bed; connections to the robot include the multi-tube air hose and the encoder cable and connections to the planning workstation is 100-FX fiber optic ethernet.

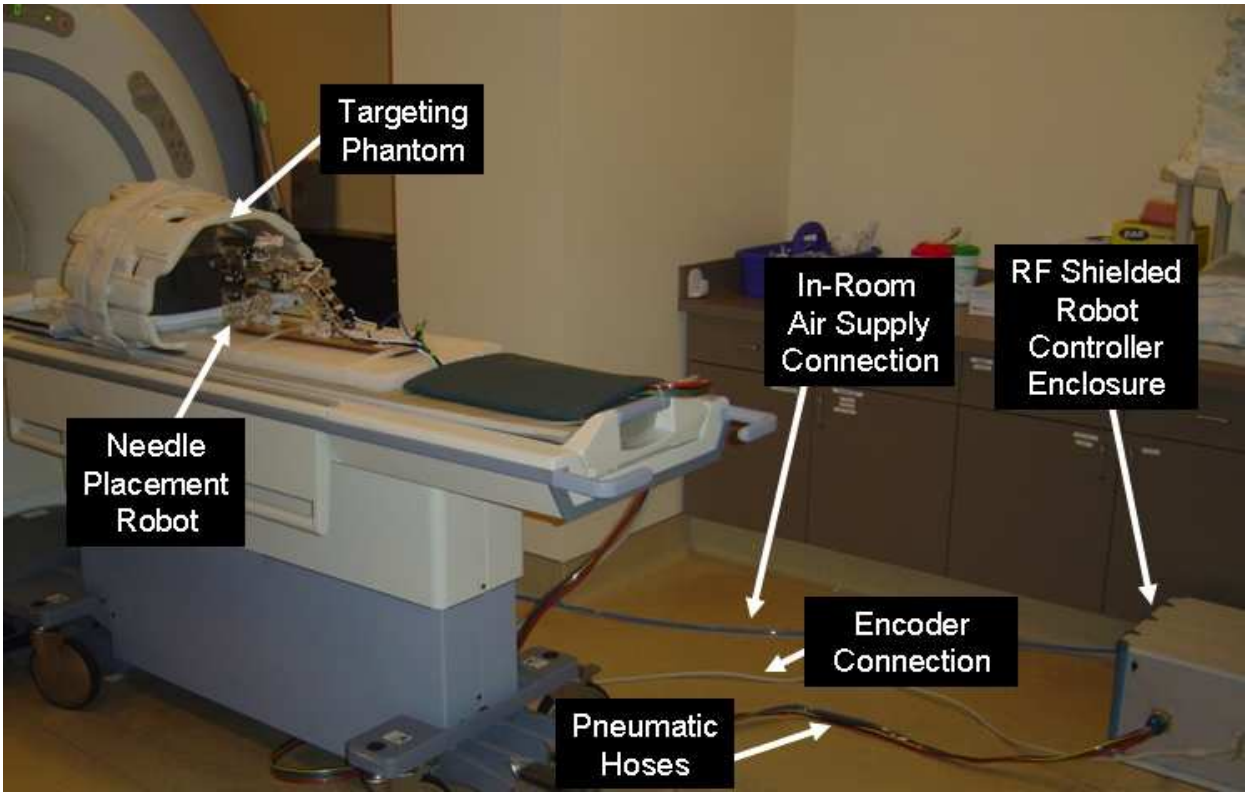

Figure 7: Configuration of robot for system evaluation trials. The robot resides on the table at a realistic relative position to the phantom. The controller operates in the room at a distance of $3m$ from the 3T MRI scanner without functional difficulties or significant image quality degradation.

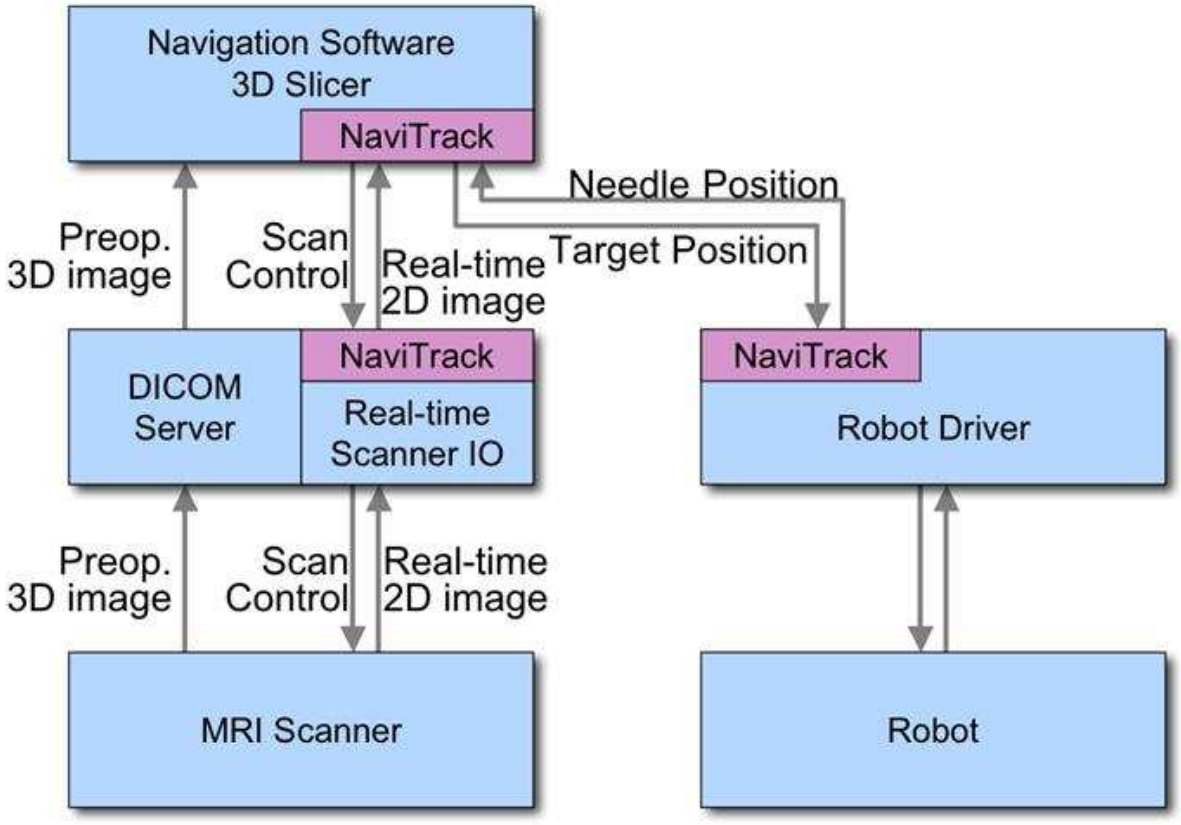

Figure 8: The diagram shows the connection and the data flow among the components. NaviTrack, an open-source device communication tool is used to exchange control, position and image data.

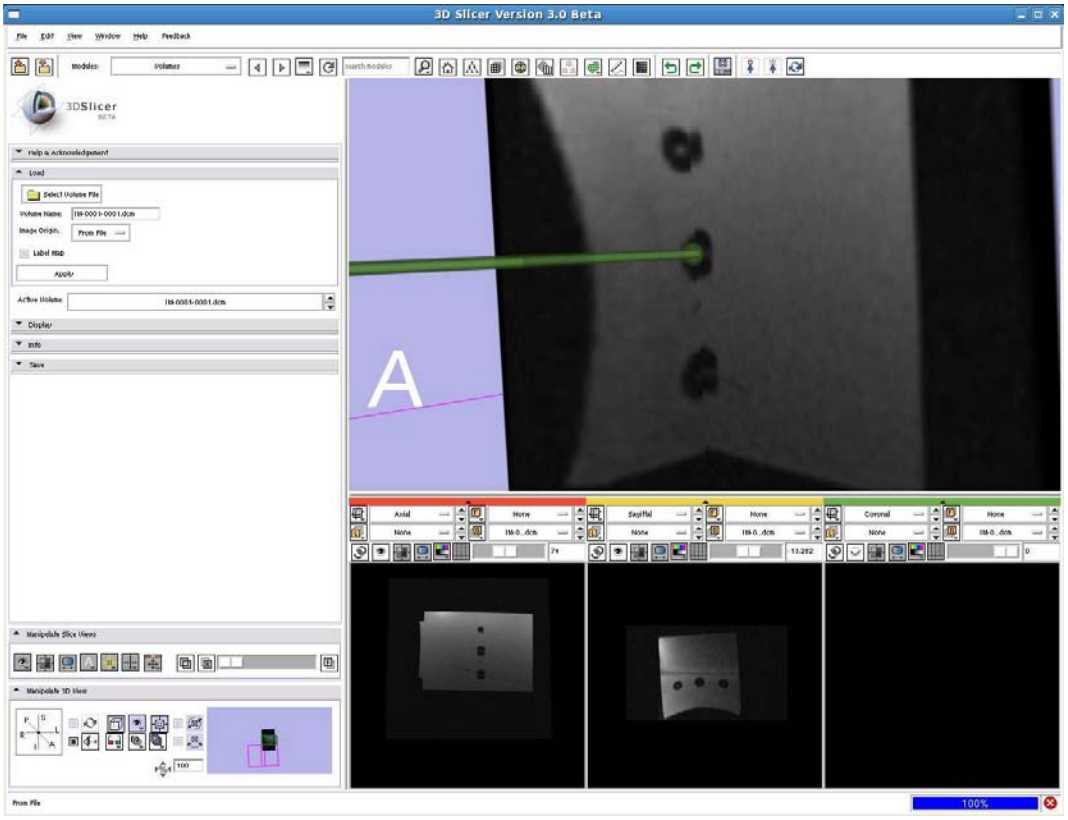

Figure 9: 3D Slicer planning workstation showing a selected target and the real-time readout of the robot's needle position. The line represents a projection along the needle axis and the sphere represents the location of the needle tip.

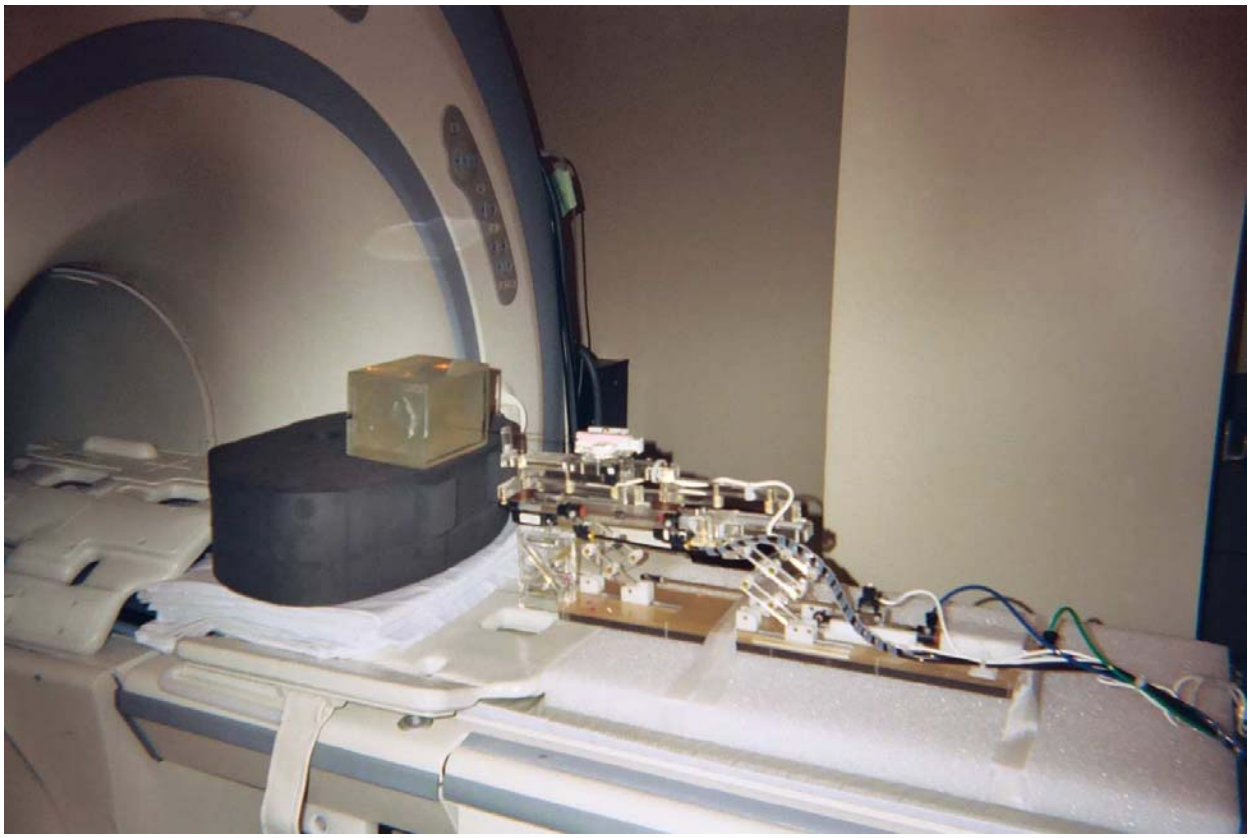

Figure 10: Robotic system performing a needle insertion into a phantom in preliminary workflow evaluation experiments. Five out of five $1cm$ targets were successfully targeted.

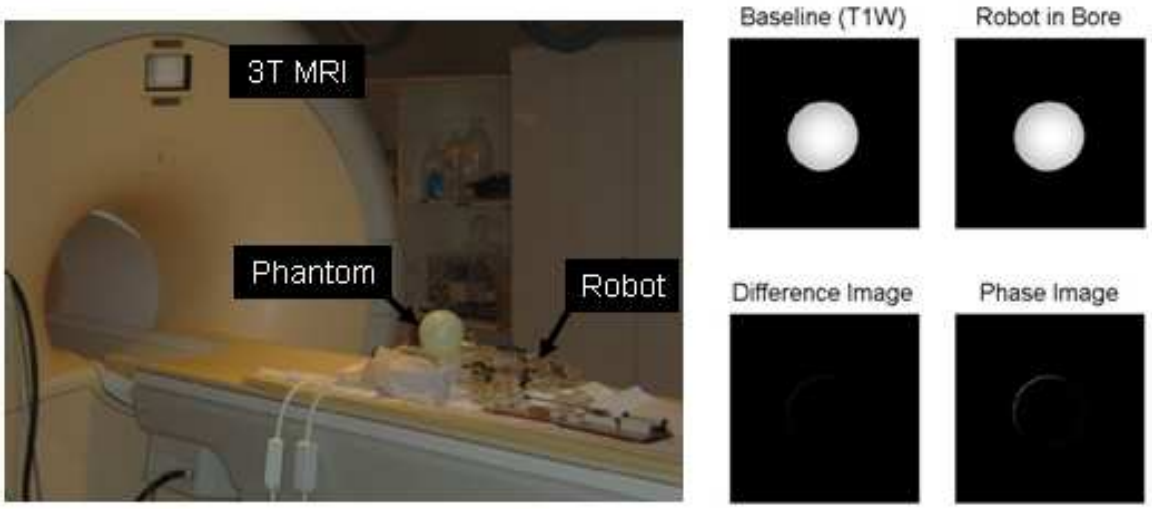

Figure 11: Configuration of the system for MRI compatibility trials. The robot is placed on the bed with the center of a spherical phantom (left) $120mm$ from the tip of the robot and the controller is placed in the scanner room near the foot of the bed. Images of the phantom taken with the T1W sequence are shown with and without the robot present (right).

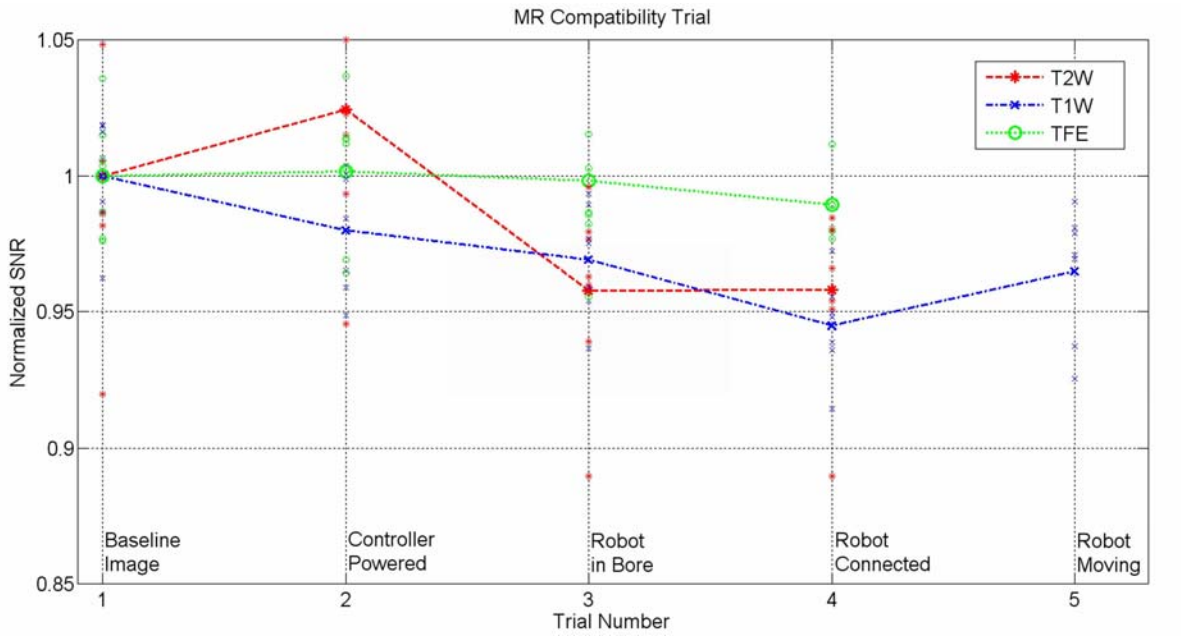

Figure 12: Qualitative measure of image quality for three standard prostate imaging protocols with the system in different configurations. Lines represent mean SNR within $25mm$ cube at center of homogeneous phantom and discrete points represent SNR in the $25mm$ square on each of seven $3mm$ slices making up the cube.

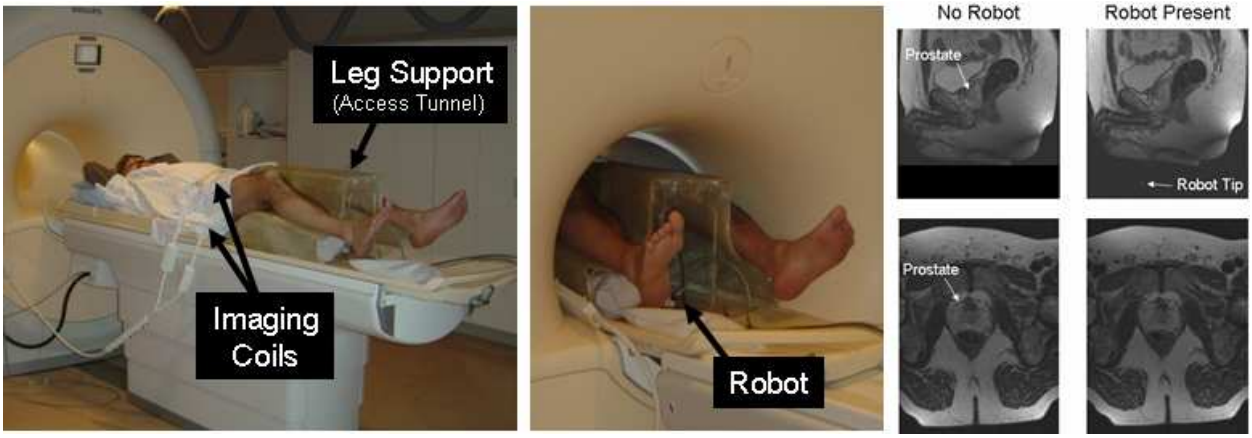

Figure 13: Qualitative analysis of prostate image quality. Patient is placed on the leg support (left) and the robot sits inside of the support tunnel inside the scanner bore (center). T2 weighted sagittal and transverse images of the prostate taken when no robot components were present and when the robot was active in the scanner (right).

Accepted for publication in the Proceedings of the International Conference on Robotics and Automation, May 2008

Pneumatically Operated MRI-Compatible Needle Placement Robot for Prostate Interventions

Gregory S. Fischer*, Iulian Iordachita*, Csaba Csoma*, Junichi Tokuda†, Philip W. Mewes†,
Clare M. Tempany†, Nobuhiko Hata† and Gabor Fichtinger‡
* Johns Hopkins University, Baltimore, MD, USA
† Brigham and Women's Hospital, Harvard University, Boston, MA, USA
‡ Queen's University, Kingston, ON, Canada
E-mail: gfischer@jhu.edu

***Abstract*— Magnetic Resonance Imaging (MRI) has potential to be a superior medical imaging modality for guiding and monitoring prostatic interventions. The strong magnetic field prevents the use of conventional mechatronics and the confined physical space makes it extremely challenging to access the patient. We have designed a robotic assistant system that overcomes these difficulties and promises safe and reliable intra-prostatic needle placement inside closed high-field MRI scanners. The robot performs needle insertion under real-time 3T MR image guidance; workspace requirements, MR compatibility, and workflow have been evaluated on phantoms. The paper explains the robot mechanism and controller design and presents results of preliminary evaluation of the system.**

I. INTRODUCTION

Each year approximately 1.5M core needle biopsies are performed, yielding about 220,000 new prostate cancer cases in the U.S. [1]. If the cancer is confined to the prostate, then low-dose-rate (LDR) permanent brachytherapy is a common treatment option; a large number (50-150) of radioactive pellets/seeds are implanted into the prostate using $15-20cm$ long 18G needles [2]. A complex seed distribution pattern must be achieved with great accuracy in order to eradicate the cancer, while minimizing radiation toxicity to adjacent healthy tissues. Transrectal Ultrasound (TRUS) is the current "gold standard" for guiding both biopsy and brachytherapy; however, TRUS-guided biopsy has a detection rate of only $20-30\%$ [3]. Furthermore, TRUS cannot effectively monitor the implant procedure as implanted seeds cannot be seen in the image. MRI seems to possess many of the capabilities that TRUS is lacking with high sensitivity for detecting prostate tumors, high spatial resolution, excellent soft tissue contrast, and volumetric imaging capabilities. However, closed-bore high-field MRI has not been widely adopted for prostate interventions because strong magnetic fields and confined physical space present formidable challenges.

The clinical efficacy of MRI-guided prostate brachytherapy and biopsy was demonstrated by D'Amico, Tempany, *et al.* at the Brigham and Women's Hospital using a 0.5T open-MRI scanner [4]. The needles were inserted manually using a guide comprising a grid of holes, with the patient in the lithotomy position, similarly to the TRUS-guided approach. Zangos *et al.* used a transgluteal approach with 0.2T MRI, but did not specifically target the tumor foci [5]. Susil *et al.* described four cases of transperineal prostate biopsy in a closed-bore scanner, where the patient was moved out of the bore for needle insertions and then placed back into the bore to confirm satisfactory placement [6]. Beyersdorff *et al.* performed targeted transrectal biopsy in a 1.5T MRI unit with a passive articulated needle-guide and have reported 12 cases of biopsy to date [7]. Robotic assistance has been investigated for guiding instrument placement in MRI, beginning with neurosurgery [8] and later percutaneous interventions [9], [10]. Chinzei *et al.* developed a general-purpose robotic assistant for open MRI [11] that was subsequently adapted for transperineal intra-prostatic needle placement [12]. Krieger *et al.* presented a 2-DOF passive, un-encoded and manually manipulated mechanical linkage to aim a needle guide for transrectal prostate biopsy with MRI guidance [13]. With the use of three active tracking coils, the device is visually servoed into position and then the patient is moved out of the scanner for needle insertion. Stoianovici *et al.* has made developments in pneumatic stepper motors and applied them toward robotic brachytherapy seed placement thus far demonstrated in training phantoms [14]. Other recent developments in MRI-compatible mechanisms include pneumatic stepping motors on a light needle puncture robot [15] and haptic interfaces for fMRI [16].

This work introduces the design of a novel computer-integrated robotic mechanism for transperineal prostate needle placement in 3T closed-bore MRI. The mechanism is capable of positioning the needle for treatment by ejecting radioactive seeds or diagnosis by harvesting tissue samples inside the magnet bore, under remote control of the physician without moving the patient out of the imaging space. This enables the use of real-time multi-parametric imaging for precise placement of needles in soft tissues. In addition to structural images, protocols for diffusion imaging and MR spectroscopy will be available intraoperatively, promising enhanced visualization and targeting of pathologies. Accurate and robust needle placement devices, navigated based on such image guidance, are becoming valuable clinical tools and have clear applications in several other organ systems.

An overview of the full system architecture, including details regarding planning software and integration of real-time MR imaging isdescribed in [17]. This paper focusses on design and evaluation of the robotic needle placement manipulator and is organized as follows: Section II describes the design requirements for the proposed device, Section III outlines details of system prototype design. Results of preliminary evaluation are presented in Section IV, with conclusions discussed in Section V.

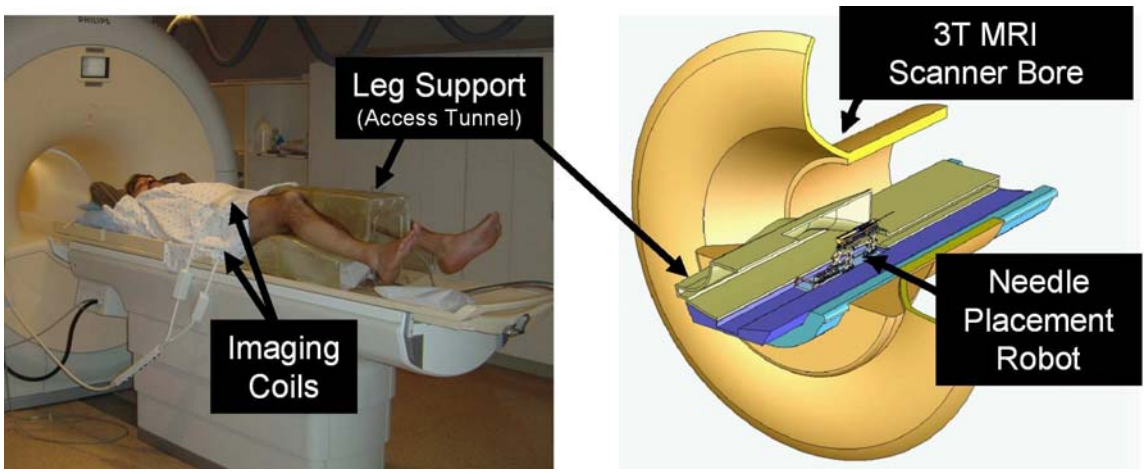

Fig. 1. Patient positioning on the leg support (left) and robot positioning within the confined space of the access tunnel (right). The robot accesses the patient's prostate through the perineal wall which rests against an opening in the superior surface of the leg rest.

II. Design Requirements

A. Workspace Analysis

The system's primary function is to accurately place needles in the prostate for the purpose of biopsy and brachytherapy seed placement. In our approach, the patient is positioned in the supine position with the legs spread and raised as shown in Fig. 1 (left). The patient is positioned in a similar configuration to TRUS-guided brachytherapy, but the MRI bore's constraint ($60cm$ diameter) requires that the legs be spread less and the knees be lower into a semi-lithotmy position. The robot operates in the confined space between the patient's legs without interference with the patient, MRI scanner components, anesthesia equipment, and auxiliary equipment present as shown in the cross-section shown in Fig. 1 (right).

The average size of the prostate is $50mm$ in the lateral direction by $35mm$ in the anterior-posterior direction by 40mm in length. The prostate volume can be approximated by an elliptical volume formula of the form $V = (.525 \times D_1 \times D_2 \times D_3)$, and the average volume is about $35cc$. Due to swelling, the volume of the prostate can also enlarge by 25% by the end of the procedure [18]. The standard $60mm \times 60mm$ perineal window of TRUS-guided brachytherapy was increased to $100mm \times 100mm$, in order to accommodate patient variability and lateral asymmetries in patient setup. In depth, the workspace is extends to $150mm$ superior of the perineal surface. Direct access to all clinically relevant locations in the prostate is not always possible with a needle inserted purely along apex-base direction due to pubic arch interference (PAI). If more than 25% of the prostate diameter is blocked (typically in prostates larger than $55cc$), then the patient is usually declined for implantation [18]. The addition of rotational alignment in the sagittal and coronal planes in the proposed system will enable the procedure to be performed on many of these patients who are usually contraindicated for brachytherapy due to PAI.

B. System Requirements

The workspace analysis allows us to derive kinematic requirements for the robot. A kinematic diagram is shown in Fig. 2; the primary motions of the base include two prismatic motions and two rotational motions upon a manual linear slide. The slide positions the robot in the access tunnel and allows fast removal for reloading brachytherapy needles or collecting harvested biopsy tissue. In addition to these base motions, application-specific motions are also required; these include needle insertion, canula retraction, needle rotation, and biopsy gun actuation. The accuracy of the individual servo controlled joints is targeted to be $0.1mm$, and the needle placement accuracy of the robot is targeted to be $0.5mm$. The overall system accuracy, however, is expected to be somewhat less when effects such as imaging resolution, needle deflection, and tissue deformation are taken into account. The specifications for the requirements of each motion are shown in Table I. The numbered motions in the table correspond to the labeled joints in the equivalent kinematic diagram shown in Fig. 2. These specifications represent a flexible system that can accommodate a large variety of patients.

C. MRI Compatibility Requirements

Design of a system operating inside the bore of a high-field 1.5 - $3T$ MRI scanner adds significant complexity since standard materials, sensors and actuators cannot be employed. In order for a device to be MR compatible, it must be MR safe and not compromise image quality. Both issues relate to the use of metals and electronics, in three respects. First, ferromagnetic materials must be avoided because they cause image artifacts and distortion, and can become dangerous projectiles. Non-ferromagnetic metals such as aluminum, brass, and titanium or high strength plastic and composite materials are therefore permissible. Second, we must prevent or limit local heating in the proximity of the patient's body. Thus the materials and structures used must be either non-conductive or free of loops and of carefully chosen lengths to avoid eddy currents and resonance. Third, we must maintain image quality, by limiting the use of conductive materials in the vicinity of the scanner's isocenter. The following section details material and component selection, with the consideration of MRI compatibility issues.

TABLE I
KINEMATIC SPECIFICATIONS

	Degree of Freedom	Motion	Requirements
1)	Gross Axial Position	1m	Manual with repeatable stop
2)	Vertical Motion	0-100mm	Precise servo control
3)	Elevation Angle	$+15°$, $-0°$	Precise servo control
4)	Horizontal Motion	$\pm$50mm	Precise servo control
5)	Azimuth Angle	$\pm 15°$	Precise servo control
6)	Needle Insertion	150mm	Manual or Automated
7)	Canula Retraction or Biopsy Gun Firing	60mm	Manual or Automated
8)	Needle Rotation	360°	Manual or Automated

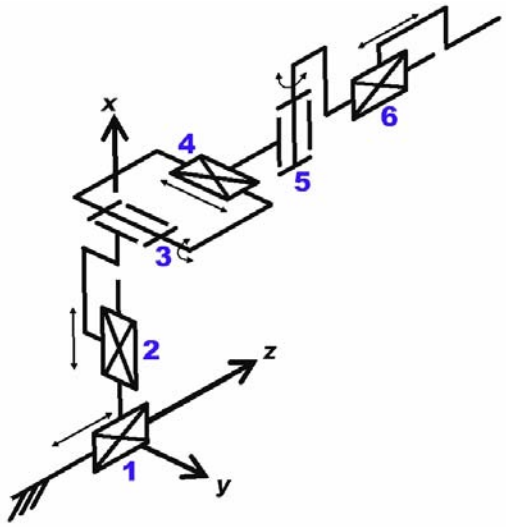

Fig. 2. Equivalent kinematic diagram of the robot - details the primary six degrees of freedom for needle insertion procedures with this manipulator. Additional application-specific end effectors may be added to provide additional DOF.

III. SYSTEM AND COMPONENT DESIGN

A. Overview

For the initial proof-of-concept system and Phase-1 clinical trials, it is not necessary to have all of the DOF listed in Table I. The first embodiment of the system provides the two prismatic motions in the axial (transverse) plane over the perineum ($DOF\#2$ and $DOF\#4$) and an encoded manual needle guide ($DOF\#6$) representing an automated high-resolution needle guide, functionally similar to the template in conventional brachytherapy. The next design iteration will produce a 4-DOF robot base with the links made out of high strength, dimensionally stable, highly electrically insulating and sterilizable plastic (e.g. Ultem or PEEK). The 4-DOF base of the manipulator design has a modular platform that allows for different end effectors to be mounted on it. The two initial end effectors will accommodate biopsy guns and brachytherapy needles. Both require an insertion phase; the former requires activating a single-acting button to engage the device and a safety lock. The latter requires an additional controlled linear motion to accommodate the cannula retraction to release the brachytherapy seeds. Sterility has been taken into consideration for the design of the end effectors. In particular, the portions of the manipulator and leg rest that come in direct contact with the patient or needle will be removable and made of materials that are suitable for sterilization. The remainder of the robot will be draped.

B. Mechanism Design

Since the robot is constructed without the use of metallic links, mechanism design is particularly important. With a proper design: the kinematics can be simplified, control can be made less complex, motions may be decoupled, actuators can be aligned appropriately and system rigidity can be increased. Based upon analysis of the workspace and the application, the following additional design requirements have been adopted:

1) Linear motion should be able to be decoupled from the rotations since the majority of procedures will not require the two rotational DOF.
2) Actuator motion should be in the axial direction (aligned with the scanner's axis, B_o) to maintain a compact profile.
3) Extension in both the vertical and horizontal planes should be telescopic to minimize the working envelope.

The four primary base degrees of freedom ($DOF\#2$-5 in Table I) are broken into two decoupled 2-DOF planar motions. In order to maintain high rigidity, planar bar mechanisms are used. Other options include cables, pulleys, gears, linear slides, leadscrews, etc.; however, these were avoided in an attempt to design a very reliable, robust, compact, and rigid system. Motion in the vertical plane includes $100mm$ of vertical travel, and up to $15°$ of positive elevation angle. This is achieved using a modified version of a scissor lift mechanism that is traditionally used for plane parallel motion. By coupling two such mechanisms as shown in Fig. 3, the two desired DOF can be achieved. Stability is increased by using a pair of such mechanisms in the rear. For purely prismatic, both slides move in unison; angulation (θ) is generated by relative motions. To aid in decoupling, the actuator for the rear slide can be fixed to the carriage of the primary motion linear drive, thus allowing one actuator to be locked when angulation is unnecessary. As shown in Fig. 3, the push rods for the front and rear motions are coupled together to maintain only translational motion in the initial prototype.

Motion in the horizontal plane is accomplished with a second planar bar mechanism. This motion is achieved by coupling two straight line motion mechanisms as shown in Fig. 4, generally referred to as Scott-Russell mechanisms. By combining two such straight-line motions, both linear and rotational motions can be realized in the horizontal plane. The choice of this design over the use of the previously described scissor-type mechanism is that this allows for bilateral motion with respect to the nominal center position. Actuation is provided by a custom, MR-compatible pneumatic cylinder that is oriented in the axial direction. Fig. 4 shows the mechanism in the 1-DOF configuration where only translation is available. This is accomplished by linking the front and rear mechanisms with a coupling link. A benefit of this deign is that it is straightforward to add the rotational motion for future designs by replacing the rigid connecting

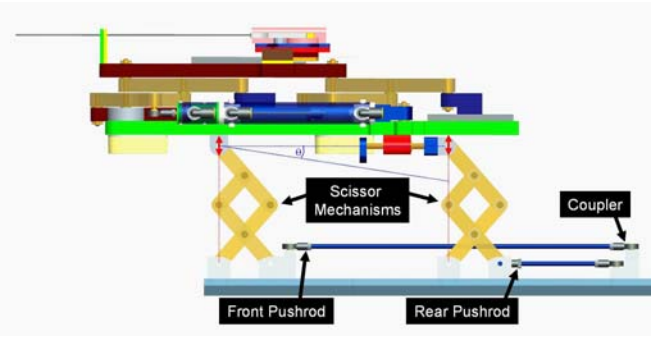

Fig. 3. Mechanism design for motion in the vertical plane. Coupling the forward and rear motion provides for vertical travel, independently moving the rear provides for elevation angle (θ) adjustment.

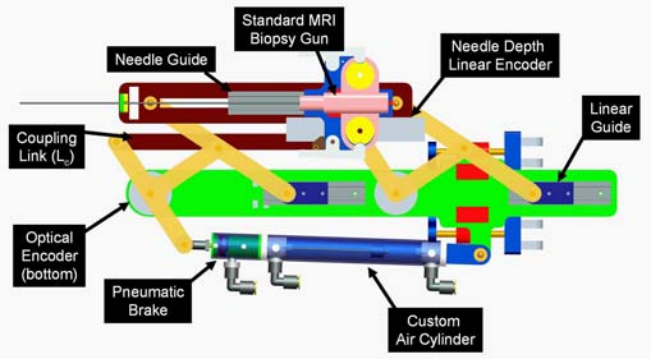

Fig. 4. Mechanism design for motion in the horizontal plane. Provides for planar parallel motion; can provide both translation and rotation by actuating rear motion independently by replacing coupling link (L_C) with a second cylinder. The attached needle guide provides accurate depth measurement during manual needle insertion. The modular needle guide can be replaced with different end effectors for other procedures.

bar (L_C) with a pneumatic cylinder. Translational motion remains decoupled when rotation is not used by ensuring that the cylinder in the connecting bar remains locked.

C. Actuator Design

The MRI environment restricts the choice of sensors and actuators. Many robots use electro-dynamic actuation, however, the very nature of an electric motor precludes its use in high-field magnetic environments. Therefore, it is necessary to: 1) use actuators that are compatible with the MR environment, or 2) to use a transmission to mechanically couple the manipulator in close proximity to the scanner to standard actuators situated outside the high field. MR compatible actuators such as piezoceramic motors have been evaluated by [19] and [11]; however, these are prone to introducing noise into MR imaging and therefore negatively impacting image quality. The latter can take the form of flexible driveshafts [13], push-pull cables, or hydraulic (or pneumatic) couplings [16].

To maintain close proximity of the actuators to the robot, alternatives to electric motors include hydraulic or pneumatic actuators. Hydraulic actuators offer the advantages of high stiffness and near-incompressible flow at the expense of speed/bandwidth, more difficult fluid connections, and the potential for leaks. Pneumatic actuators offer relatively high speed, large availability of components, and readily available compressed air supply at the expense of decreased rigidity and less straightforward control due to the compressibility of air and the relatively large non-linear friction forces in the cylinder. Further, portability of the system and ease of connections contradicts the closed-system nature of hydraulic actuators. Pneumatic cylinders are the actuator of choice for this robot.

Although pneumatic actuation seems ideal for MRI, most standard pneumatic cylinders are not suitable for use in MRI. Custom MR compatible pneumatic cylinders have been developed for use with this robot. The cylinders are based upon Airpel $9.3mm$ bore cylinders [1]. These cylinders were chosen because the cylinder bore is made of glass and the piston and seals are made of graphite. This design has two main benefits; the primary components are suitable for MRI and they inherently have very low friction (as low as $1g$). In collaboration with the manufacturer, we developed the cylinders shown in Fig. 5 that are entirely nonmetallic except for the brass shaft. The cylinders can handle up to $100psi$ ($6.9bar$) and therefore can apply forces up to $46.8N$. In addition to moving the robot, it is important to be able to lock it in position to provide a stable needle insertion platform. Pneumatically operated, MR compatible brakes have been developed for this purpose. The brakes are compact units that attach to the ends of the previously described cylinders as shown in Fig. 4 and clamp down on the rod. The design is such that the fail-safe state is locked and applied air pressure releases a spring-loaded collet to enable motion. The brakes are disabled when the axis is aligned and applied when the needle is to be inserted or an emergency situation arises.

There are three basic valve types that are used for servo control of a cylinder: 1) High-bandwidth on-off valves, 2) Proportional flow spool valves, and 3)Proportional pressure regulator valves. Proportional pressure regulators were the valve of choice for this robot because they allow for direct control of the pressure, thus the force, on the robot. This is

[1] Airpel E9 Anti-stiction Air Cylinder - http://www.airpel.com

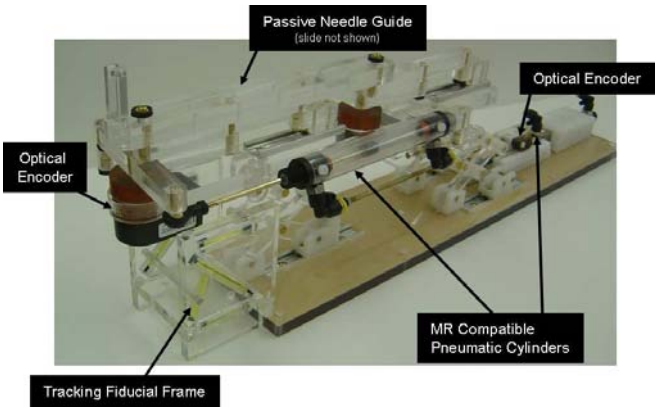

Fig. 5. Robotic needle placement mechanism with two active DOF and one passive, encoded needle insertion. Actuation is by custom, MR compatible pneumatic cylinder and position sensing by optical encoders. Dynamic global registration is achieved with the attached tracking fiducial.

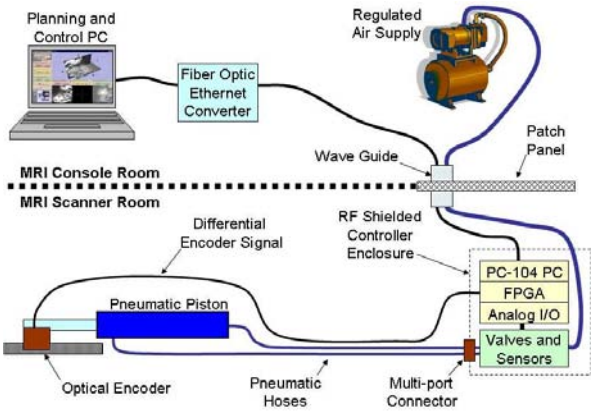

Fig. 6. Diagram representing controller connection to a single representative actuator. All low-level control takes place inside of the scanner room; embedded computer and valves are in an enclosure placed in the scanner room at the foot of the bed and robot actuators and position sensors are inside of the scanner bore. The controller communicates with high-level planning software through a fiber optic connection.

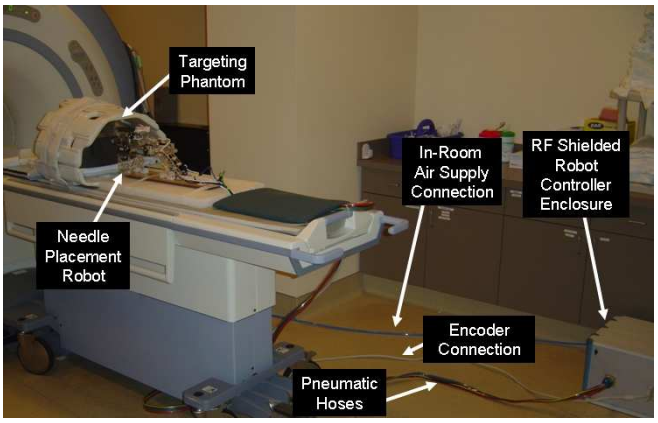

Fig. 7. Configuration of robot for system evaluation trials. The robot resides on the table at a realistic relative position to the phantom. The controller operates in the room at a distance of only $2.5m$ from the 3T MRI scanner without functional difficulties or significant image quality degradation.

an advantage because it aids in controller design and also has the inherent safety of being able to limit applied pressure to a prescribed amount.

Most pneumatic valves are operated either directly by a solenoid coil or indirectly by a small pilot valve that is actuated by a solenoid coil. Unfortunately, as with electric motors, the very nature of a solenoid coil is a contraindication for its use in an MR environment. With pneumatic control, it is essential to limit the distance from the valve to the cylinder on the robot; thus it is important to use valves that are safe and effective in the MR environment. The robot uses piezoelectrically actuated proportional pressure valves[2] that do not use traditional solenoid coil, thus permitting their use near MRI. A pair of these valves provide a differential pressure of $\pm 100psi$ on the cylinder piston for each actuated axis. A further benefit of piezoelectrically actuated valves is the rapid response time ($4ms$). Thus, by using piezoelectric valves the robot's bandwidth can be increase significantly by limiting tubing lengths and increasing controller update rate.

D. Position Sensing

Standard methods of position sensing that are generally suitable for pneumatic cylinders include: linear potentiometers, linear variable differential transformers (LVDT), capacitive sensors, ultrasonic sensors, magnetic sensors, laser sensors, optical encoders, and cameras (machine vision). Most of these sensing modalities are not practical for use in an MR environment. However, there are two methods that do appear to have potential: 1) linear optical encoders and 2) direct MRI image guidance.

Standard optical encoders[3] have been thoroughly tested in a 3T MRI scanner for functionality and induced effects in the form of imaging artifacts as described in [17]. The encoders have been incorporated into the robot and have performed without any stray or missed counts; the imaging artifact is confined locally to within 2-$5cm$ from the encoder. This is sufficient because the robot is designed to distance the sensors from the prostate imaging volume.

Direct MRI-based image guidance shows great promise for high-level control, safety and verification, and for robot-scanner registration; however, the refresh rate and resolution is not sufficient for use in low-level servo control of a robot joint. Examples of practical methods of robot tracking are discussed in [13]. Dynamic global registration between the robot and scanner is provided by passive tracking fiducials on the robot base and is described in detail in [20]. The rigid structure of the the fiducial frame is made up of seven rigid glass tubes with $3mm$ inner diameters that are filled with contrast extracted from MR Spot fiducials (Beekley, Bristol, CT). The rods are placed on three faces of a $60mm$ cube as shown in Fig. 5, and any arbitrary MR image slicing through all of the rods provides the full 6-DOF pose of the frame, and thus the robot, with respect to the scanner. Thus, by locating the fiducial attached to the robot, the transformation between patient coordinates (where planning is performed) and the robot's needle driver is known. The end effector location is then calculated from the kinematics based on the encoder positions and compared with the location in the MR images of the fiducials attached to the needle driver shown in Fig. 5.

E. Robot Controller Hardware

MRI is very sensitive to electrical signals passing in and out of the scanner room. For that reason and to minimize the distance between the valves and the robot, the robot controller is placed inside of the scanner room. An overview of the connections and breakdown of component locations is shown in Fig. 6. The controller comprises an EMI shielded enclosure that sits at the foot of the scanner bed as shown in Fig. 7; the controller has proved to be able to operate within $2.5m$ of the scanner bore. Inside of the enclosure is an embedded computer with analog I/O for interfacing with valves and pressure sensors and an FPGA module for

[2]Hoerbiger-Origa PRE-U piezo valve- http://www.hoerbigeroriga.com

[3]EM1-500 linear and E5D-1250 rotary encoder modules with PC5 differential line driver - US Digital, Vancouver, Washington

interfacing with joint encoders. Also in the enclosure are the piezoelectric servo valves, piezoelectric brake valves and pressure sensors. The distance between the servo valves and the robot is minimized, thus maximizing the bandwidth of the pneumatic actuators. The expected bandwidth is $100Hz$. Control software on the embedded PC, provides for low level joint control and an interface to interactive scripting and higher level trajectory planning. Low-level control software is implemented on the embedded computer inside the robot controller enclosure inside the scanner room. The computer runs Linux using the Real Time Application Interface (RTAI)[4] kernel extension to allow for the accurate clock necessary for PC-based servo control.

Pneumatic connections from the robot interface to the manipulator that is sitting on the bed in the scanner bore are simplified with a multi-port pneumatic connector and bundled air tubing that can accommodate up to 10 connections in a single plug. Encoder connections are made using a single standard 68 conductor twisted pair shielded cable that mates to the robot axes through a custom circuit board on the robot with individual connectors per axis as in Fig. 7. Communication with the planning and control workstation sitting in the MR console room is through a fiber optic ethernet connection. No electrical connections pass out of the scanner room limiting, thus significantly limiting the MR imaging interference.

F. Interface Software

Interface with the robot is via 3D Slicer-based[5] software GUI running on the planning laptop PC in the scanner's console room and is described in detail in [21]. A DICOM server running on the planning workstation retrieves images from the scanner console. Both preoperative and intra-operative images can be loaded into the application for procedure planning and for intra-operative guidance. The Slicer workstation calculates the location of the robot with respect to the patient coordinate system based upon images of the tracking fiducial described in Section III-D. A target and entry point are chosen on the planning PC, and the robot is sent the coordinates and aligns the needle guide appropriately. In the current system, the needle is inserted manually while the needle position is monitored by an encoded slider and displayed in real-time on the display. Real-time MR images ($0.5Hz$) will be used during the insertion phase to ensure the target is reached. The reason for a keeping a human in the loop is to increase the safety of the needle insertion, and to allow for the live MRI images to help monitor progress. Fig. 8 shows the planning software with an MR image of the phantom loaded and the real-time feedback of the robot is used to generate the needle axis superimposed on the MR image.

IV. Results

The first iteration of the needle placement robot has been constructed and is operational; all mechanical, electrical, communications, and software issues have been resolved. The current state of the manipulator is two actuated DOF (vertical and horizontal) with an encoded passive needle insertion stage as shown in Fig. 5. Evaluation of the robot is in three distinct phase: 1) evaluation of the MR compatibility of the robot, 2) evaluation of the workspace and workflow, and 3) evaluation of the localization and placement accuracy.

[4]RTAI - http://www.rtai.org

[5]3D Slicer - http://www.slicer.org

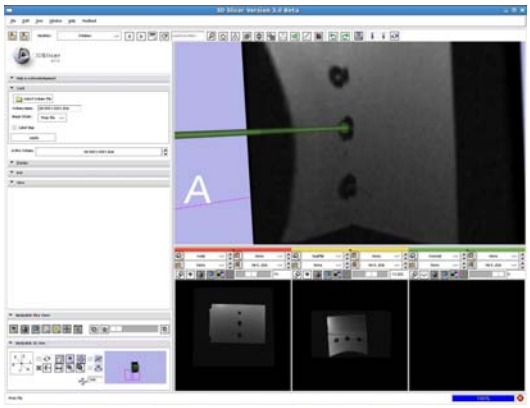

Fig. 8. 3D Slicer planning workstation showing a selected target and the real-time readout of the robot's needle position. The line represents a projection along the needle axis and the sphere represents the location of the needle tip.

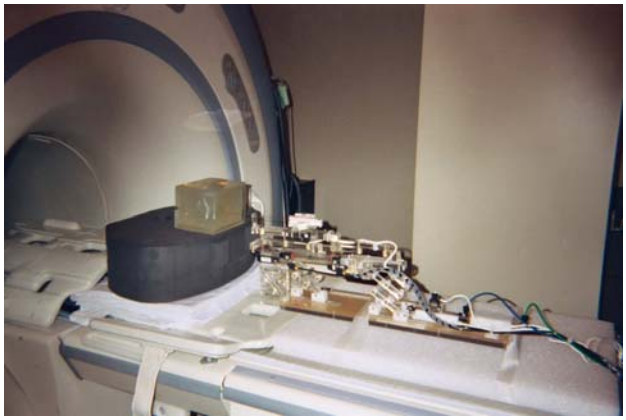

Fig. 9. Robotic system performing a needle insertion into a phantom in preliminary workflow evaluation experiments. Five out of five $1cm$ targets were successfully targeted.

The MR compatibility of the system is thoroughly evaluated in [17]. Using standard prostate imaging sequences (T1, T2 and TSE) the maximum loss in average signal to noise ration (SNR) was shown to be 5%. Qualitatively, prostate images were captured while the robot was operational is there is no readily identifiable loss of image quality when the robot is present.

The required workspace was evaluated prior to construction and has been confirmed by imaging patients in the appropriate position on the leg rest and verifying that all extents of the prostate are reachable. Further studies of this are underway where volunteers are imaged on the leg rest in the appropriate semi-lithotomy position and the prostate and anatomical constraints are analyzed.

Accuracy assessment is broken into two parts: localization and placement. These two must be distinguished, especially

in many medical applications. In prostate biopsy, it is essential to know exactly where a biopsy comes from in order to be able to forma treatment plan if cancer is located. In brachytherapy treatment, radioactive seed placement plans must be made to avoid cold spots where irradiation is insufficient; by knowing where seeds are placed, the treatment plan can be updated in real-time. Based on encoder resolution, localization accuracy of the robot is better than $0.1mm$ in all directions. Positioning accuracy is dependent on the servo pneumatic control system. With the controller hardware complete and a preliminary controller based upon standard PID techniques in place, the robot can be positioned within about $5mm$; this represents the approximate targeting resolution in traditional ultrasound-guided transperineal prostate interventions. This accuracy is expected to be improved significantly as we refine the controller design. Development of novel pneumatic control architecture is underway, and the goal is for the target positioning accuracy to approach the resolution of the encoders. Experiments with sliding mode control algorithms that are more robust to the high friction of the mechanism show great promise, and we intend to achieve $0.1mm$ positioning accuracy per axis.

V. CONCLUSIONS AND FUTURE WORKS

We have developed an MRI-compatible manipulator and the support system architecture that can be used for needle placement in the prostate for biopsy and brachytherapy procedures. The robot has been designed such that it will operate in the confined space between the patient's legs inside a leg rest/tunnel in a high-field, closed bore MRI scanners. The configuration allows the use of diagnostic MRI scanners in interventional procedures; there is no need for open or large bore scanners that often are difficult to come by and sacrifice image quality. Evaluation of the system's workspace, MR-compatibility, workflow, and user interface has been very positive. All of the primary elements of the system are now in place; further refinement of the control system and interface software are in progress.

The next phase of this work focusses on generating clinical-grade system and preparing for Phase-1 clinical trials. The initial application will be prostate biopsy, followed later by brachytherapy seed placement. The design of the manipulator allows for treatment of patients that may have otherwise been denied such treatment because of contraindications such as significant pubic arch interference. The robot, controller and/or system architecture are generally applicable to other MR robotic applications. We intend to deploy a platform not only for prostate biopsy and brachytherapy, but also for injections, thermal ablation, and optical sensing modalities under MR image guidance.

ACKNOWLEDGMENTS

This work was supported by NSF EEC-97-31478, NIH BRP RO1-CA111288-01, NIH/NIBIB R01-EB002963-01, NIH U41-RR019703, and CDMRP PCRP Fellowship W81XWH-07-1-0171.

REFERENCES

[1] A. Jemal, R. Siegel, E. Ward, T. Murray, J. Xu, and M. Thun, "Cancer statistics, 2007," in *CA Cancer J Clin*, vol. 57(1), pp. 43–66, 2007.

[2] J. C. Blasko, T. Mate, J. Sylvester, P. Grimm, and W. Cavanagh, "Brachytherapy for carcinoma of the prostate," in *Semin Radiat Oncol*, vol. 12(1), pp. 81–94, 2002.

[3] M. K. Terris, E. M. Wallen, and T. A. Stamey, "Comparison of midlobe versus lateral systematic sextant biopsies in detection of prostate cancer," in *Urol Int*, vol. 59, pp. 239–242, 1997.

[4] A. V. D'Amico, C. M. Tempany, R. Cormack, N. Hata, M. Jinzaki, K. Tuncali, M. Weinstein, and J. Richie, "Transperineal magnetic resonance image guided prostate biopsy," in *J Urol*, vol. 164(2), pp. 385–7, 2000.

[5] S. Zangos, K. Eichler, K. Engelmann, M. Ahmed, S. Dettmer, C. Herzog, W. Pegios, A. Wetter, T. Lehnert, M. G. Mack, and T. J. Vogl, "MR-guided transgluteal biopsies with an open low-field system in patients with clinically suspected prostate cancer: technique and preliminary results," in *Eur Radiol*, vol. 15(1), pp. 174–82, 2005.

[6] R. C. Susil, K. Camphausen, P. Choyke, E. R. McVeigh, G. S. Gustafson, H. Ning, R. W. Miller, E. Atalar, C. N. Coleman, and C. Ménard, "System for prostate brachytherapy and biopsy in a standard 1.5 T MRI scanner," in *Magnetic Resonance in Medicine*, vol. 52, pp. 683–6873, 2004.

[7] D. Beyersdorff, A. Winkel, B. Hamm, S. Lenk, S. A. Loening, and M. Taupitz, "MR imaging-guided prostate biopsy with a closed MR unit at 1.5 T," in *Radiology*, vol. 234, pp. 576–581, 2005.

[8] K. Masamune, E. Kobayashi, Y. Masutani, M. Suzuki, T. Dohi, H. Iseki, and K. Takakura, "Development of an MRI-compatible needle insertion manipulator for stereotactic neurosurgery," in *J Image Guid Surg*, vol. 1(4), pp. 242–8, 1995.

[9] A. Felden, J. Vagner, A. Hinz, H. Fischer, S. O. Pfleiderer, J. R. Reichenbach, and W. A. Kaiser, "ROBITOM-robot for biopsy and therapy of the mamma," in *Biomed Tech (Berl)*, vol. 47, pp. 2–5, 2002.

[10] E. Hempel, H. Fischer, L. Gumb, T. Hhn, H. Krause, U. Voges, H. Breitwieser, B. Gutmann, J. Durke, M. Bock, and A. Melzer, "An MRI-compatible surgical robot for precise radiological interventions," in *CAS*, pp. 180–191, Apr. 2003.

[11] K. Chinzei, N. Hata, F. A. Jolesz, and R. Kikinis, "MR compatible surgical assist robot: system integration and preliminary feasibility study," in *MICCAI*, vol. 1935, pp. 921–933, Oct. 2000.

[12] S. P. DiMaio, S. Pieper, K. Chinzei, G. Fichtinger, C. Tempany, and R. Kikinis, "Robot assisted percutaneous intervention in open-MRI," in *MRI Symp*, p. 155, 2004.

[13] A. Krieger, R. C. Susil, C. Menard, J. A. Coleman, G. Fichtinger, E. Atalar, and L. L. Whitcomb, "Design of a novel MRI compatible manipulator for image guided prostate interventions," in *IEEE TBME*, vol. 52, pp. 306–313, Feb. 2005.

[14] M. Muntener, A. Patriciu, D. Petrisor, D. Mazilu, H. Bagga, L. Kavoussi, K. Cleary, and D. Stoianovici, "MRI compatible robotic system for fully automated brachytherapy seed placement," in *J. Urology*, vol. 68, pp. 1313–7, 2006.

[15] E. Taillant, J. Avila-Vilchis, C. Allegrini, I. Bricault, and P. Cinquin, "CT and MR Compatible Light Puncture Robot: Architectural Design and First Experiments," in *MICCAI*, vol. 3217, pp. 145–152, 2004.

[16] R. Gassert, R. Moser, E. Burdet, and H. Bleuler, "MRI/fMRI-Compatible Robotic System With Force Feedback for Interaction With Human Motion," in *T. Mech.*, vol. 11(2), pp. 216–24, Apr. 2006.

[17] G. S. Fischer, S. P. DiMaio, I. Iordachita, and G. Fichtinger, "Development of a Robotic Assistant for Needle-Based Transperineal Prostate Interventions in MRI," in *MICCAI*, pp. 425–433, Nov. 2007.

[18] K. Wallner, J. Blasko, and M. Dattoli, *Prostate Brachytherapy Made Complicated, 2nd Ed.* SmartMedicine Press, 2001.

[19] H. Elhawary, A. Zivanovic, M. Rea, B. Davies, C. Besant, D. McRobbie, N. de Souza, I. Young, and M. Lamprth, "The Feasibility of MR-Image Guided Prostate Biopsy Using Piezoceramic Motors Inside or Near to the Magnet Isocentre," in *MICCAI*, pp. 519–526, Nov. 2006.

[20] S. P. DiMaio, E. Samset, G. S. Fischer, I. Iordachita, G. Fichtinger, F. Jolesz, and C. Tempany, "Dynamic MRI Scan Plane Control for Passive Tracking of Instruments and Devices," in *MICCAI*, pp. 50–58, Nov. 2007.

[21] P. W. Mewes, J. Tokuda, S. P. DiMaio, G. S. Fischer, C. Csoma, D. G. Gobbi, C. M. Tempany, G. Fichtinger, and N. Hata, "An Integrated MRI and Robot Control Software System for an MRI-compatible Robot in Prostate Intervention," in *IEEE ICRA*, Apr. 2008.

Robotic Assistant for Transperineal Prostate Interventions in 3T Closed MRI

Gregory S. Fischer[1], Simon P. DiMaio[2],
Iulian I. Iordachita[1], and Gabor Fichtinger[1]

[1] Center for Computer Integrated Surgery, Johns Hopkins University, USA
[gfischer,iordachita,gaborf]@jhu.edu,
[2] Surgical Planning Lab, Harvard University, USA
simond@bwh.harvard.edu.

Abstract. Numerous studies have demonstrated the efficacy of image-guided needle-based therapy and biopsy in the management of prostate cancer. The accuracy of traditional prostate interventions performed using transrectal ultrasound (TRUS) is limited by image fidelity, needle template guides, needle deflection and tissue deformation. Magnetic Resonance Imaging (MRI) is an ideal modality for guiding and monitoring such interventions due to its excellent visualization of the prostate, its sub-structure and surrounding tissues. We have designed a comprehensive robotic assistant system that allows prostate biopsy and brachytherapy procedures to be performed entirely inside a 3T closed MRI scanner. We present a detailed design of the robotic manipulator and an evaluation of its usability and MR compatibility.

1 Introduction

Core needle biopsy is considered the definitive method of diagnosis for prostate cancer, and each year approximately 1.5M core needle biopsies are performed, yielding about 220,000 new prostate cancer cases in the U.S. [1]. When cancer is confined to the prostate, low-dose-rate permanent brachytherapy, where 50-150 radioactive pellets/seeds are placed into the prostate, is a common treatment option. A complex seed distribution pattern must be achieved, while minimizing radiation toxicity to adjacent healthy tissues. Transrectal Ultrasound (TRUS) is the current "gold standard" for guiding biopsy and brachytherapy. However, current TRUS-guided biopsy has a detection rate of 20-30% [2] and TRUS-guided brachytherapy cannot readily visualize seed placement in the US images. Further, the template in TRUS-guided procedures limits the placement precision and the ability to effectively guide oblique insertions. MRI has high sensitivity for detecting prostate tumors, high spatial resolution, excellent soft tissue contrast and multiplanar volumetric imaging capabilities, making it an ideal modality for guiding and monitoring such procedures.

The clinical efficacy of MRI-guided prostate biopsy and brachytherapy was demonstrated by D'Amico, Tempany, et al. using a 0.5T open-MRI scanner to plan and monitor transperineal needle placement [3]. Needles were manually

N. Ayache, S. Ourselin, A. Maeder (Eds.): MICCAI 2007, Part I, LNCS 4791, pp. 425–433, 2007.

inserted using a plastic template, with the patient oriented in the lithotomy position, similarly to the TRUS-guided approach. Beyersdorff et al. performed targeted transrectal biopsy in 1.5T MRI with a passive articulated needle guide [4]. Krieger et al. present a 2-DOF passive, un-encoded and manually manipulated mechanical linkage to aim a needle guide for transrectal prostate biopsy with MRI guidance [5]. Robotic assistance has been investigated for guiding instrument placement in MRI, beginning with neurosurgery [6] and later percutaneous interventions [7]. Chinzei et al. developed a general-purpose robotic assistant for open MRI [8] that was subsequently adapted for transperineal intra-prostatic needle placement [9]. Stoianovici et al. has made developments in pneumatic stepper motors and applied them to robotic brachytherapy seed placement [10]. Other MRI-compatible mechanisms include pneumatic motors for a light puncture robot [11] and haptic interfaces for fMRI [12].

The patient is in the prone postion in [4] and [5], which make preoperative and intraoperative image fusion difficult; further, the transrectal approach precludes using commercially available endorectal imaging coils. The system presented in [10] is very complex and places the the patient in the fetal position, again preventing the pre- and intra-operative images from aligning and challenges traditional patient positioning for both MR imaging and and brachytherapy. The presented robotic system is of simpler design, lower cost, and above all, incorporates ergonomics suited for prostate biopsy and brachytherapy by allowing the patient to retain the supine (semi-lithotomy) pose used for preoperative imaging.

This work presents the design and development of a comprehensive robot-assisted system for transperineal prostate needle placement in 3T closed-bore MRI. The system integrates an image-based target planning interface, a robotic placement mechanism that allows for remote manipulation of the needle in the magnet bore without moving the patient out of the imaging space, as well as robot and needle tracking for navigation and control.

2 Methods

2.1 System Layout and Architecture

We have developed a comprehensive computer-integrated needle placement system to accurately target planned tissue sites by minimizing needle misplacement effects. The complete system comprises two main modules, integrated with high-field diagnostic MRI scanners. First is a visualization, planning and navigation system, and second is a robotic assistant for needle placement. The architecture of this system is outlined in Fig. 1.

In blocks **a** and **b**, 3D Slicer software (www.slicer.org) fuses multimodality pre-operative images with pre-procedural MR images for procedure planning. Kinematics of the needle trajectories are evaluated subject to anatomical constraints and constraints of the needle placement mechanism. Device and needle navigation are shown in blocks **c**, **d** and **e**, which are enclosed in a loop that represents device/needle positioning and sensing/localization. Blocks **d** and **e** guide the needle positioning device; an image-based servo loop tracks the needle

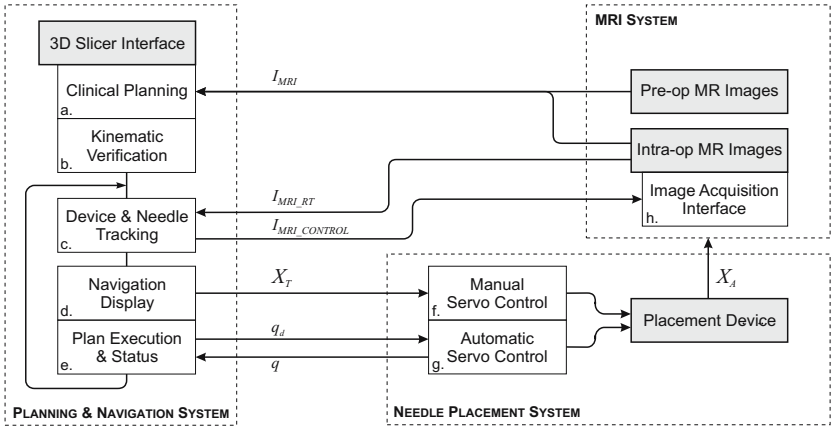

Fig. 1. System architecture (left) and component distribution (right)

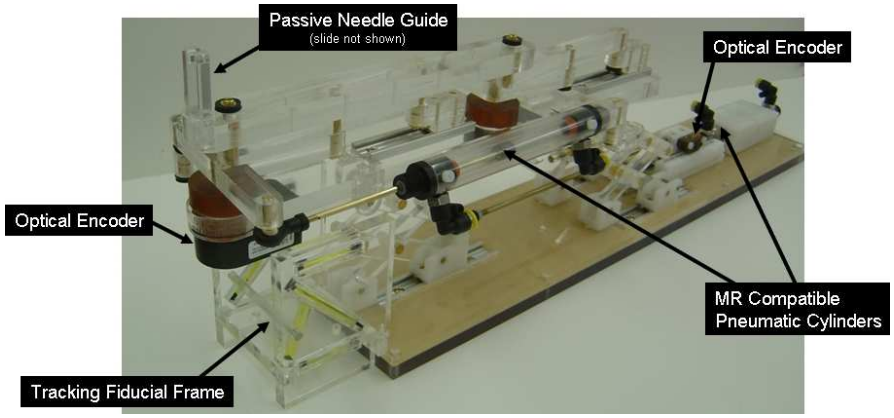

Fig. 2. Robot manipulator capable of two actuated DOFs with manual needle insertion. The tracking fiducial frame at the front of the robot is used for locating the robot in the scanner coordinate system.

and provides real-time images along it's axis to help detect and limit needle and tissue deflection effects. Blocks **f** and **g** are the robotic mechanism that provides remote operation of the needle while the patient is within the magnet bore.

2.2 Mechanical Design

The patient is positioned in the supine position such that their legs are placed on a leg support that provides a "tunnel" of access to the perineum. This creates a well defined workspace at the patient's perineum, while maintaining a compact profile to prevent interference with the patient, the scanner and adjacent equipment. The focus of the first phase is to bring MR guidance to the same degrees of freedom (DOF) available in traditional TRUS template-guided procedures. The kinematic requirements are $100mm$ in the vertical and horizontal directions and passive needle insertion guide with an encoded travel of $120mm$. To mimic the traditional TRUS procedure and also for increased safety, needle insertion

is performed manually along the needle guide that is aligned by the robot. Already incorporated in the mechanical design, but not actuated in the present prototype system are two additional DOF; 15° of rotation in the vertical and horizontal planes will help avoid pubic arch interference that may typically be a contraindication using traditional techniques. This will be particularly important since space constraints of the MR scanner prevent positioning the patient in the full lithotomy position; thus, lowering the pubic arch and increasing the likelyhood of interference.

Vertical motion is generated by a modified scissor lift mechanism. Two such mechanisms actuated independently provide vertical motion and elevation angle. Horizontal motion is generated by a second planar bar mechanism that rests upon the vertical stage. Prismatic and rotational motions can be realized by coupling two such straight-line motion mechanisms. For both stages, actuation is provided by custom pneumatic cylinders described in Section 2.3. The actuators are oriented along the bore axis (B_0), thus reducing the overall width significantly. The complete assembly is shown in Fig. 2. Sterility is insured by making the top-most portion of the passive needle guide removable and draping the remainder of the robot. Further, the tissue contacting surface of the leg rest will be removable and sterilizable.

2.3 Actuation and Control

Pneumatic actuators were chosen because they offer relatively high speed and power for their weight and provide for compact means of actuation at the mechanism. They also do not require involved setup or allow the risk of fluid leakage, which is a sterility concern, associated with hydraulic systems. Servo control of the cylinders is provided by piezoelectrically actuated pressure regulator valves with switching times under $4ms$ (Hoerbiger-Origa Tecno Valve, Altenstadt, Germany). Custom MR compatible pneumatic cylinders are made with glass bores, graphite pistons, brass shafts and plastic housings (Made in collaboration with Airpel, Norwalk, CT). Pneumatic brakes are attached to each cylinder in order to lock and maintain needle position/orientation during needle insertion. They are unlocked by applying air pressure.

The robot uses linear strip optical encoders for the vertical motion stage and rotary encoders on the horizontal motion stage. Encoders were thoroughly tested in 3T MRI for functionality and imaging compatibility (US Digital EM1 with PC5 differential driver, Vancouver, Washington). Functionality was evaluated by confirming that no encoder counts were lost as the mechanism periodically oscillated in the bore of the scanner during imaging. Imaging compatibility was confirmed by monitoring the effect on the MR images under standard prostate imaging protocols as described later in Section 3.1.

A controller sitting in the MR scanner room near the foot of the bed provides low level control of the robot. Inside of the EMI shielded enclosure is an embedded computer with analog I/O for interfacing with valves and pressure sensors and an FPGA module for interfacing with joint encoders. Also in the enclosure are piezoelectric servo valves, piezoelectric brake valves and pressure

sensors. The short distance between the servo valves and the robot is minimized, thus maximizing the bandwidth of the pneumatic actuators. The expected bandwidth is 100Hz. Control software on the embedded PC provides for low-level joint control and an interface to interactive scripting and higher-level trajectory planning. Communication with the planning and control workstation is through a fiberoptic ethernet connection.

Dynamic global registration between the robot and scanner is provided by passive tracking fiducials on the robot base and is described in detail in [13]. The rigid structure of the the fiducial frame is made up of seven rigid glass tubes with $3mm$ inner diameters that are filled with contrast extracted from MR Spot fiducials (Beekley, Bristol, CT). The rods are placed on three faces of a $60mm$ cube as shown in Fig. 2, and any arbitrary MR image slicing through all of the rods provides the full 6 DOF pose of the frame, and thus the robot, with respect to the scanner. Thus, by locating the fiducial attached to the robot, the transformation between patient coordinates (where planning is performed) and the robot's needle driver is known.

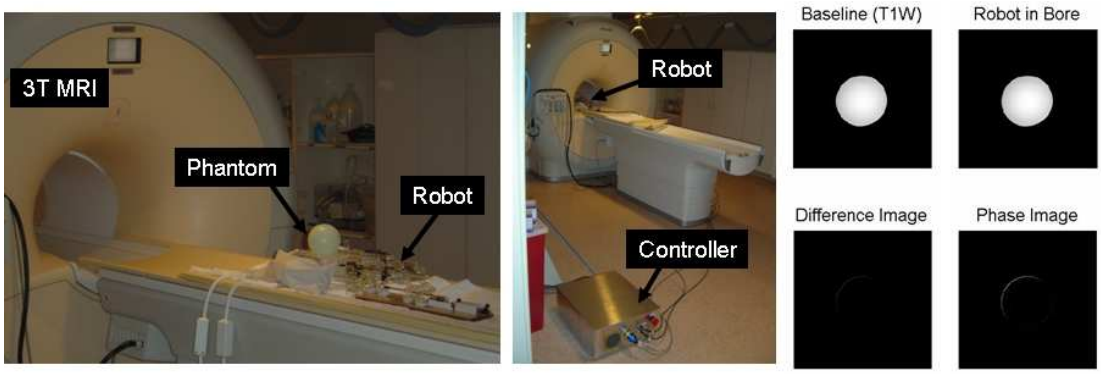

Fig. 3. Experimental setup for compatibility trials. The robot is placed on the bed alongside a spherical MR phantom (left) and the controller is placed in the scanner room near the foot of the bed(center). Images of the spherical phantom taken with the T1W sequence are shown with and without the robot present; the square at the center represents the field of view used for SNR calculations. Below them are the corresponding difference and phase images (right).

3 Results

3.1 MR Compatibility

MR Compatibility includes three main elements: 1) safety, 2) preserving image quality, and 3) maintaining functionality. Safety issues such as RF heating are minimized by isolating the robot from the patient, avoiding wire coils, and avoiding resonances in components of the robot; ferrous materials are completely avoided to prevent the chance of a projectile. Image quality is maintained by again avoiding ferromagnetic materials, limiting conductive materials near the

imaging site, and avoiding RF sources. Pneumatic actuation and optical sensing, as described in Section 2.3, preserve full functionality of the robot in the scanner.

Evaluation and verification of the MR compatibility of the system was a primary goal of this work. Compatibility was evaluated on a 3T Philips Achieva scanner. A $10cm$ spherical MR phantom was placed at the isocenter and the robot placed such that the tip was at a distance of $120mm$ from the center of the phantom (a realistic depth from perineum to prostate) as shown in Fig. 3 (left). The phantom was imaged using three standard prostate imaging protocols: 1) **T2W TSE**: T2 weighted turbo spin echo (28cm FOV, 3mm slice, TE=90ms, TR=5600ms, 2) **T1W FFE**: T1 weighted fast field gradient echo (28cm FOV, 3mm slice, TE=2.3ms, TR=264ms) and 3) **TFE (FGRE)**: "Real time" turbo field gradient echo (28cm FOV, 3mm slice, TE=10ms, TR=26ms). A baseline scan with each sequence was taken of the phantom with no robot components using round flex coils similar to those often used in prostate imaging. The following imaging series were taken in each of the following configurations: 1) Phantom only, 2) Controller in room and powered, 3) Robot placed in scanner bore, 4) Robot electrically connected to controller and 5) Robot moving during imaging (only with T1W imaging). For each step, all three imaging sequences were performed and both magnitude and phase images were collected.

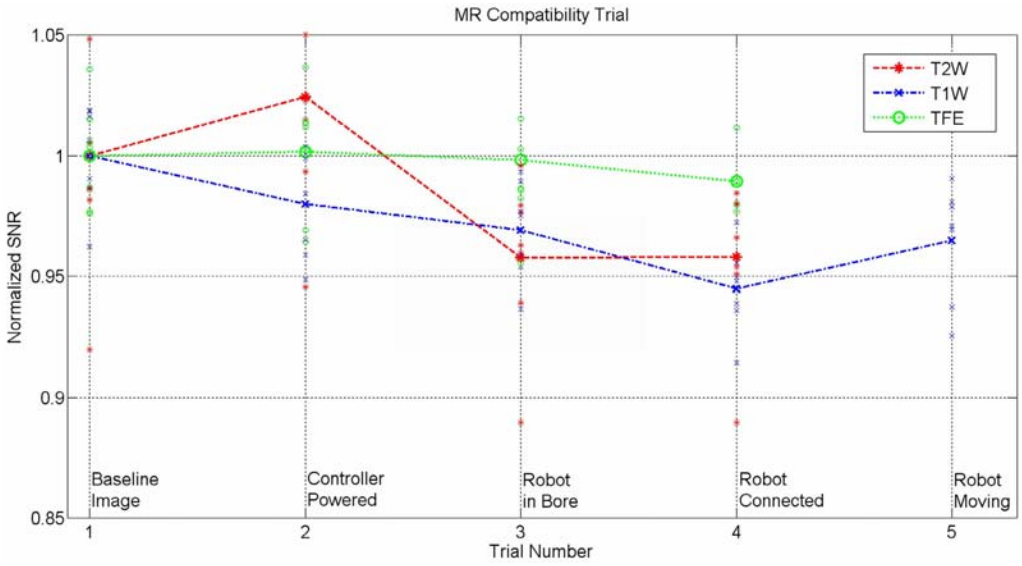

Fig. 4. Signal to noise ratio for three standard prostate imaging protocols with the system in different configurations. Lines represent mean SNR within 25mm cube at center of homogeneous phantom and discrete points represent SNR in the 25mm square on each of seven $3mm$ slices making up the cube.

The effect on image quality was judged by computing the signal to noise ratio (SNR). SNR of an MR image can be calculated with several techniques; we chose to define it as the mean signal in a $25mm$ square at the center of the homogeneous sphere divided by the standard deviation of the signal in that same region as shown in Fig. 3 (right). The SNR of the magnitude images was normalized by

the value for the baseline image, thus limiting any bias in choice of calculation technique or location. SNR was evaluated at seven slices (representing 25mm width) at the center of the sphere for each of the three imaging sequences. The points in the graph in Fig. 4 show the SNR in the phantom for seven $3mm$ thick slices for each sequence at each configuration. The lines represent the average SNR in the $25mm$ cube at the center of the spherical phantom for each sequence at each configuration. When the robot was operational, the reduction in SNR of the $25mm$ cube at the phantom's center for these pulse sequences was 5.5% for **T1W FFE**, 4.2% for **T2W TSE** and 1.1% for **TFE (FGRE)**. Further qualitative means of evaluating the effect of the robot on image quality are obtained by examining prostate images taken both with and without the robot present. Fig. 5 (right) shows images of the prostate of a volunteer placed in the scanner bore on the leg rest.

3.2 System Integration

To evaluate the overall layout and workflow, the robot was placed in the bore inside of the leg rest with a volunteer as shown in Fig. 5 (left). Round flex receiver coils were used for this trial; endorectal coils can be used for clinical case to obtain optimal image quality. There was adequate room for a patient and the robot was able to maintain its necessary workspace.

Co-registration of the robot to the scanner was performed using the base tracking fiducial described in Section 2.3 that is shown in Fig. 2. Images of the robot's tracking fiducial provide the location of the robot base in the scanner's coordinate system with an RMS accuracy of $0.14mm$ and 0.37^o as described in [13]. Joint encoding provides end effector localization resolution of better that $0.01mm$ and $0.1mm$ for horizontal and vertical motions, respectively. In free space, the needle tip localization accuracy with respect to the MR images is expected to be better than $0.25mm$ and 0.5^o.

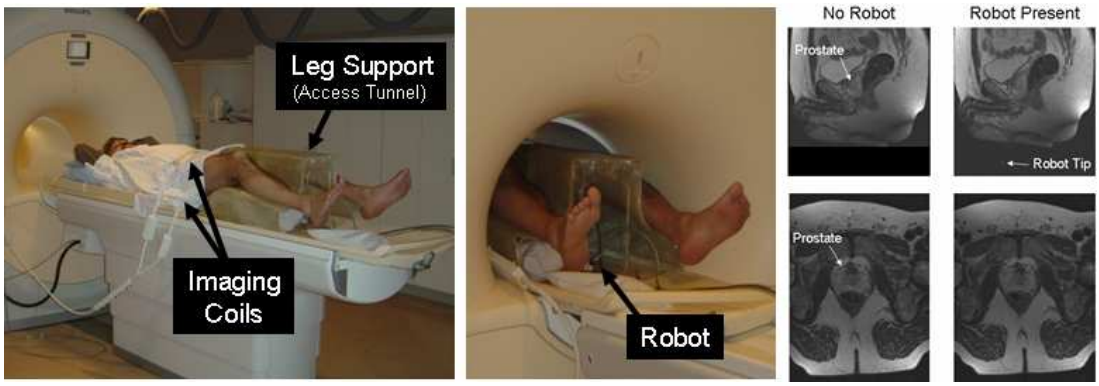

Fig. 5. Qualitative analysis of prostate image quality. Patient is placed on the leg support (left) and the robot sits inside of the support tunnel inside the scanner bore (center). T2 weighted sagittal and transverse images of the prostate taken when no robot components were present and when the robot was active in the scanner (right).

4 Discussion

MRI-guidance promises high quality, rapid, volumetric, multimodality imaging capabilities, but presents significant engineering challenges due to the harsh electromagnetic environment and tight spatial constraints in the scanner bore. We have developed a prototype robotic system for precisely targeting prostate tissue under realtime MR guidance. The current system provides the 2-DOF plus insertion of traditional TRUS-guided procedures with finer spatial resolution and image-based guidance. Needle placement accuracy can be improved from the $5mm$ grid that is standard today.

We have shown the system to be MR compatible under standard prostate imaging sequences, with sufficient accuracy for guiding prostate biopsy and brachytherapy procedures. Localization accuracy of the tracking fiducial that is attached to the robot and its application to visual servoing and dynamic scan plane control are described in our companion paper [13]. Detailed analysis of the true needle insertion error of the complete system in phantom studies, and ultimately animal and cadaver trials, is forthcoming. The next generation system will incorporate additional rotational DOFs such that pubic arch interference can be avoided, thus increasing the eligible population for these procedures. This work is also of relevance to the development of systems specialized for other organ systems and diseases that require targeted needle placement inside an MRI scanner.

This work was supported by NIH 1R01CA111288, CDMRP PCRP Fellowship W81XWH-07-1-0171, and NSF EEC-9731748.

References

1. Jemal, A., Siegel, R., Ward, E., Murray, T., Xu, J., Smigal, C., Thun, M.: Cancer statistics, 2006. CA Cancer J. Clin. 56(2), 106–130 (2004)
2. Terris, M.K., et al.: Comparison of mid-lobe versus lateral systematic sextant biopsies in detection of prostate cancer. Urol Int. 59, 239–242 (1997)
3. D'Amico, A.V., Tempany, C.M., Cormack, R., Hata, N., et al.: Transperineal magnetic resonance image guided prostate biopsy. J. Urol. 164(2), 385–387 (2000)
4. Beyersdorff, D., Winkel, A., Hamm, B., et al.: MRI-guided prostate biopsy with a closed MR unit at 1.5 T. Radiology 234, 576–581 (2005)
5. Krieger, A., Susil, R.C., Menard, C., Coleman, J.A., Fichtinger, G., Atalar, E., Whitcomb, L.L.: Design of a novel MRI compatible manipulator for image guided prostate interventions. IEEE TBME 52, 306–313 (2005)
6. Masamune, K., Kobayashi, E., Masutani, Y., Suzuki, M., Dohi, T., Iseki, H., Takakura, K.: Development of an MRI-compatible needle insertion manipulator for stereotactic neurosurgery. J. Image Guid. Surg. 1(4), 242–248 (1995)
7. Hempel, E., Fischer, H., Gumb, L., et al.: An MRI-compatible surgical robot for precise radiological interventions. In: CAS, pp. 180–191 (2003)
8. Chinzei, K., Hata, N., Jolesz, F.A., Kikinis, R.: MR compatible surgical assist robot: system integration and preliminary feasibility study. In: Delp, S.L., DiGoia, A.M., Jaramaz, B. (eds.) MICCAI 2000. LNCS, vol. 1935, pp. 921–933. Springer, Heidelberg (2000)

9. DiMaio, S.P., Pieper, S., Chinzei, K., Fichtinger, G., Tempany, C., Kikinis, R.: Robot assisted percutaneous intervention in open-MRI. In: MRI Symp. p. 155 (2004)
10. Muntener, M., Patriciu, A., Petrisor, D., Mazilu, D., Bagga, H., Kavoussi, L., Cleary, K., Stoianovici, D.: MRI compatible robotic system for fully automated brachytherapy seed placement. J. Urology 68, 1313–1317 (2006)
11. Taillant, E., Avila-Vilchis, J., Allegrini, C., Bricault, I., Cinquin, P.: CT and MR Compatible Light Puncture Robot: Architectural Design and First Experiments. In: Barillot, C., Haynor, D.R., Hellier, P. (eds.) MICCAI 2004. LNCS, vol. 3217, pp. 145–152. Springer, Heidelberg (2004)
12. Gassert, R., Moser, R., Burdet, E., Bleuler, H.: MRI/fMRI-Compatible Robotic System With Force Feedback for Interaction With Human Motion. T. Mech. 11(2), 216–224 (2006)
13. DiMaio, S., Samset, E., Fischer, G., Iordachita, I., Fichtinger, G., Jolesz, F., Tempany, C.: Dynamic MRI Scan Plane Control for Passive Tracking of Instruments and Devices. In: Ayache, N., Ourselin, S., Maeder, A. (eds.) MICCAI 2007. LNCS, vol. 4792, pp. 50–58. Springer, Heidelberg (2007)